

meso-Aryl Phenanthroporphyrins: Synthesis and Spectroscopic Properties

Hai-Jun Xu,^[a] John Mack,^[b] Ana B. Descalzo,^[c, d] Zhen Shen,^{*[a]} Nagao Kobayashi,^{*[b]}
Xiao-Zeng You,^[a] and Knut Rurack^{*[c]}

Abstract: The successful synthesis of tetraphenyltetraphenanthroporphyrin (TPTPhenP; **5a**) in 2006 under modified Rothemund–Lindsey conditions yielded a tetraphenyl porphyrinoid with a B band redshifted to an unprecedented 576 nm. Radially symmetric fused-ring expansion of tetraphenylporphyrin with phenanthrene moieties results in very deep saddling due to steric crowding and very marked redshifts of the Q and B (or Soret) porphyrinoid absorption bands. The extent to which the TPTPhenP structure can be further modified is explored, and the optical properties of TPTPhenPs are analyzed

based on a perimeter model approach that makes use of time-dependent DFT calculations and magnetic circular dichroism spectroscopy and also based on a detailed analysis of the fluorescence emission. Attempts to introduce substituents at the *ortho* and *meta* positions of the *meso*-phenyl groups and to insert a central metal proved unsuccessful. The synthesis of a series of TPTPhenPs with strong electron-with-

drawing (–CN, –NO₂) and -donating (–CH₃, –N(CH₃)₂) substituents at the *para* positions of the *meso*-phenyl rings is reported. Marked redshifts of the main spectral bands were consistently observed. The most pronounced spectral changes were observed with –N(CH₃)₂ groups (**5i**) due to a marked destabilization of the HOMO, which has large MO coefficients on the *meso*-carbon atoms. Protonation of **5i** at both the ligand core and at the –N(CH₃)₂ groups resulted in unprecedented Q₀₀ band absorption at wavelengths greater than 1200 nm.

Keywords: charge transfer • circular dichroism • dyes/pigments • porphyrinoids • protonation

Introduction

The study of redshifted porphyrinoid chromophores has attracted considerable attention in recent years because of their potential use as photosensitizers in photodynamic therapy (PDT),^[1] as fluorescent probes for the recognition of

cationic or anionic analytes,^[2] and as dyes for applications in nonlinear optics (NLO),^[3] optical limiting,^[4] opto-electronic devices,^[5] and solar-energy conversion.^[6] A redshift of the absorption and emission bands of porphyrins can usually be achieved through an extension of the π -conjugation system. A number of different approaches have been adopted over the last decade to achieve this, including the introduction of *meso*-alkynyl substituents,^[7] an increase in the number of core pyrrole rings to form sapphyrins, hexaphyrins, octaphyrins, and so on,^[8] coplanar polymerization of porphyrins,^[9] the expansion of the π system with exocyclic rings,^[10,11] and conformational distortions due to steric crowding of peripheral substituents.^[12,13] Although the fusion of exocyclic rings at the β -pyrrole positions is probably the most obvious strategy for modifying the electronic and optical properties of the π system on this basis, only limited redshifts have been observed upon substitution with fused benzene rings.^[10] The radially symmetric addition of a second set of benzo groups to form tetra-[2,3]naphthoporphyrin (TNP) from tetrabenzoporphyrin (TBP) (Scheme 1) results in only a minor redshift of the B (or Soret) band from 433 to 439 nm.^[14,15] Spence and Lash have demonstrated that the introduction of peripheral acenaphthalene rings has a far larger impact, and that further redshifts are observed when phenyl substituents are added at the *meso*-carbon atoms.^[16] They reported that the B band of the doubly protonated form of tetraacenaphthoporphyrin (TANPH₂²⁺) in CHCl₃ shifts significantly to the red from 528 nm^[17] to around 565 nm in the case of *meso*-tetraphenyl-

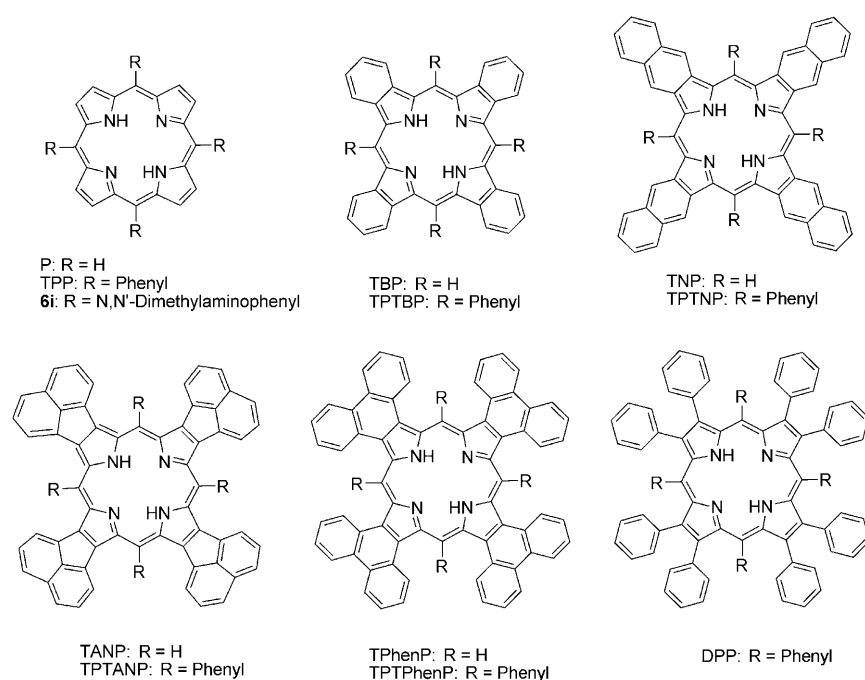
[a] Dr. H.-J. Xu, Prof. Z. Shen, Prof. X.-Z. You
State Key Laboratory of Coordination Chemistry
Nanjing National Laboratory of Microstructures
School of Chemistry and Chemical Engineering
Nanjing University, Nanjing 210093 (P.R. China)
Fax: (+86)25-8331-4502
E-mail: zshen@nju.edu.cn

[b] Dr. J. Mack, Prof. N. Kobayashi
Department of Chemistry, Graduate School of Science
Tohoku University, Sendai 980, 8578 (Japan)
Fax: (+81)22-795-7719
E-mail: nagaok@m.tohoku.ac.jp

[c] Dr. A. B. Descalzo, Dr. K. Rurack
Fachgruppe 1.5, BAM Bundesanstalt
für Materialforschung und -prüfung
Richard-Willstätter-Strasse 11, 12489 Berlin (Germany)
Fax: (+49)30-8104-1157
E-mail: knut.rurack@bam.de

[d] Dr. A. B. Descalzo
Present address: Departamento de Química Orgánica
Facultad de Ciencias Químicas
Universidad Complutense de Madrid
Avda. Complutense s/n, 28040 Madrid (Spain)

Supporting information for this article is available on the WWW under <http://dx.doi.org/10.1002/chem.201002596>.



Scheme 1. The molecular structures of porphyrinoid compounds discussed in this paper including porphyrin (P), tetraphenylporphyrin (TPP), *meso*-tetrakis(4-*N,N*-dimethylaminophenyl)porphyrin (**6i**), tetrabenzoporphyrin (TBP), tetraphenyltetrabenzoporphyrin (TPTBP), tetranaphthoporphyrin (TNP), tetraphenyltetranaphthoporphyrin (TPTNP), tetraacenaphthoporphyrin (TANP), tetraphenyltetraacenaphthoporphyrin (TPTANP), tetraphenanthroporphyrin (TPhenP), tetraphenyltetraphenanthroporphyrin (TPTPhenP, **5a**), and dodecaphenylporphyrin (DPP). For title compounds **5a–i**, see Scheme 2.

tetraacenaphthoporphyrin (TPTANPH₂²⁺).^[16] The role of *meso* substitution clearly extends beyond an enhancement of the solubility properties^[18] in this context.

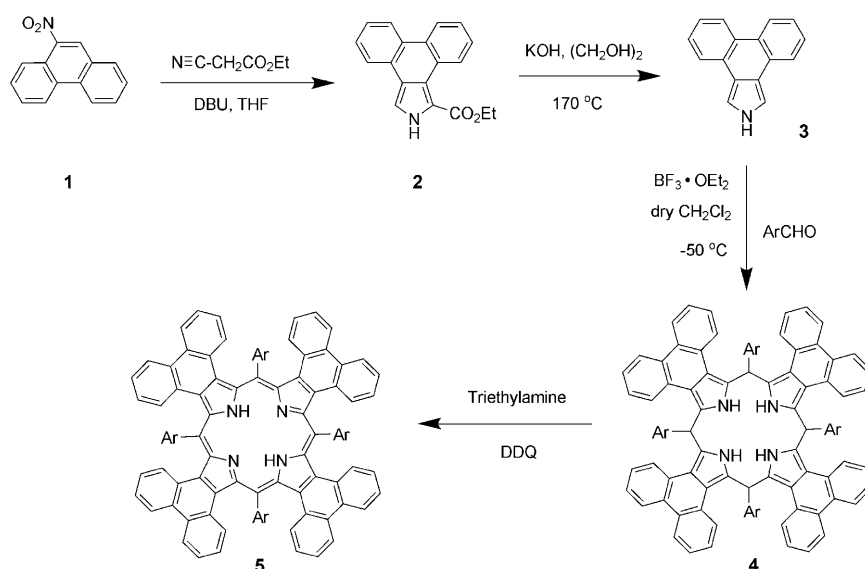
Mack et al.^[19] recently demonstrated—based on an application of Michl's perimeter model^[20] to the magnetic circular dichroism (MCD) spectroscopic analysis and theoretical calculations of a wide range of radially symmetric zinc porphyrinoids—that key trends observed in the spectral properties of porphyrinoids are largely determined by the relative energies of the four frontier π MOs associated with Gouterman's 4-orbital model.^[21] These MOs retain the nodal properties and hence the orbital angular momentum properties of a parent hydrocarbon polyene associated with the inner perimeter of the ligand. Saddled porphyrinoids such as ZnTPTANP exhibit large redshifts in the B-band region due to limited configurational interaction between the B and higher-energy π - π^* states. A key issue faced by the use of TPTANP in near-infrared (NIR) dye applications is that the forbidden and allowed nature of the Q and B bands^[21] results in relatively weak Q₀₀-band absorption. Building on this earlier research, our aim has been to introduce structural perturbations to the porphyrin π system, which modify the energies of the frontier π MOs in a predictable manner, so that rationally designed porphyrinoids can be synthesized with markedly redshifted and relatively intense Q bands.

The next logical step was to build on recent research by the Lash and Luk'yanets groups on the *meso*-tetraaryl substitution of tetraacenaphthoporphyrins^[16,18] and tetra-

[2,3]naphthoporphyrins^[15] by extending this approach to tetraphenanthroporphyrin (TPhenP) since this can be expected to yield a porphyrinoid with a still higher degree of ligand nonplanarity. Although TPhenP was successfully prepared some years ago,^[17,22] the preparation of *meso*-tetrasubstituted tetraphenanthroporphyrins initially proved unsuccessful under normal Lindsey porphyrin condensation conditions^[16] due to the steric hindrance between the *meso*-aryl substituents and the relatively bulky phenanthrene rings (Scheme 1). Recently, we were able to synthesize *meso*-tetraaryltetraphenanthroporphyrin (TPTPhenP, **5a**) based on a modification to Lindsey's method.^[22] In this paper, we explore the effect of modifying the aryl substituents of TPhenPs by preparing a range of TPTPhenP compounds including *meso*-(4-halogeno-

tetraphenyl) derivatives (**5c–f**) and newly synthesized compounds with strongly electron-donating and -withdrawing groups at the *para* position of the *meso*-phenyl rings (**5b**, **5g–i**; Scheme 2). A detailed analysis of the electronic structures and optical spectroscopy of these compounds is carried out based on an application of Michl's perimeter model.^[20]

Electronic structure of porphyrinoids: Many of the key breakthroughs in understanding the electronic structures of porphyrinoids have been based on the application of MCD spectroscopy.^[23] It currently is not possible to calculate MCD spectra by using commercially available DFT-based software packages. Older semiempirical approaches continue to play a major role in the analysis of MCD spectra, since they provide a readily accessible conceptual framework for the experimentalist that can enable the prediction of key trends in the spectral properties and thus facilitate the rational design of porphyrinoids for practical applications. Moffitt^[24] and Michl^[20] demonstrated that the relative intensities of the major electronic absorption bands of aromatic π systems can be successfully described in terms of perturbations to the structure of a high-symmetry parent hydrocarbon (C₁₆H₁₆²⁻ in the case of metal tetrapyrrole porphyrinoid complexes, or C₁₈H₁₈ for free-base compounds). The nodal patterns of the π -system MOs are retained even when the symmetry of the cyclic perimeter is modified (Figure 1 and Figure S10 in the Supporting Information). As a consequence, there is an M_L = 0, ± 1 , ± 2 , ± 3 , ± 4 , ± 5 , ± 6 ,



Scheme 2. Scheme for the preparation of **5a** (Ar = C₆H₅), **5b** (Ar = 4-Me-C₆H₄), **5c** (Ar = 4-F-C₆H₄), **5d** (Ar = 4-Cl-C₆H₄), **5e** (Ar = 4-Br-C₆H₄), **5f** (Ar = 4-I-C₆H₄), **5g** (Ar = 4-NC-C₆H₄), **5h** (Ar = 4-O₂N-C₆H₄) and **5i** (Ar = 4-Me₂N-C₆H₄). Compounds **5j** (Ar = 3-O₂N-C₆H₄) and **5k** (Ar = 2,5-Cl₂-C₆H₃) could not be obtained on this basis.

± 7 , 8 sequence in ascending energy terms in the π MOs of metal porphyrinoids in an analogous manner to the $M_L=0$, ± 1 , ± 2 , 3 π MO sequence that forms the basis of the aromatic properties of benzene. Within the band nomenclature of Gouterman's 4-orbital model,^[21] there is an electronically allowed B transition and a forbidden Q transition that links the frontier $M_L=\pm 4$, ± 5 π MOs based on $\Delta M_L=\pm 1$ and ± 9 β transitions, respectively. Electromagnetic radiation can rotate a maximum of once per wavelength, so only $\Delta M_L=0$, ± 1 transitions are electric-dipole-allowed. The incorporation of four pyrrole rings into the parent perimeter to form planar metal porphyrin (MP) complexes reduces the symmetry from D_{16h} to D_{4h} , which is further lowered to D_{2h} in the context of free-base compounds. The LUMO and LUMO+1 of MP complexes retain $M_L=\pm 5$ nodal patterns (Figure 1) and are orbitally degenerate in the context of metal complexes ($1e_g^*$) with only a slight splitting typically predicted in the context of free-base compounds ($1b_{2g}^*$ and $1b_{3g}^*$).^[25] The MOs associated with the HOMO of the parent perimeter can be readily identified based on their $M_L=\pm 4$ nodal patterns and are symmetry split under both D_{4h} ($1a_{1u}$ and $1a_{2u}$) or D_{2h} ($1a_u$ and $1b_{1u}$) symmetry. In the context of porphyrins, these two MOs remain accidentally near degenerate, and the orbital angular momentum (OAM) properties of the lowest-lying $\pi-\pi^*$ excited states therefore remain relatively close to those of the parent hydrocarbon perimeter. Since there are only minor splittings of the doubly degenerate HOMO and LUMO of the parent perimeter (referred to as the $\Delta HOMO$ and $\Delta LUMO$ values by Michl^[20]; Figure 2), the Q bands that lay at lower energy remain almost fully forbidden and there is typically very weak electronic absorption intensity in the Q-band region based primarily on vibrational borrowing from the allowed B_{00} bands.^[26] When a

structural perturbation introduces a large $\Delta HOMO$ and/or $\Delta LUMO$ value, there is a mixing of the allowed and forbidden properties of the Q and B bands and a marked intensification of the Q band, which as a consequence can become the dominant spectral feature for some porphyrinoids such as the phthalocyanines.^[25]

MCD spectroscopy^[23] can be used to identify the main electronic bands and to derive structural information that cannot be obtained from UV/Vis absorption and NMR spectra alone, since the signs and intensities of the spectral bands are determined by the OAM properties of the ground and excited states. Analysis of the MCD spectrum is based on intensity mechanisms described

by the Faraday \mathcal{A}_1 , \mathcal{B}_0 , and \mathcal{C}_0 terms.^[23] Since the main $\pi\rightarrow\pi^*$ bands of D_{4h} -symmetry MPs arise from transitions out of orbitally nondegenerate $1a_{1u}$ and $1a_{2u}$ MOs into an orbitally degenerate $1e_g^*$ LUMO, there is a nondegenerate ground state ($^1A_{1g}$) and orbitally degenerate excited states (1E_u). The MCD intensity mechanism is based on the differential absorbance of left and right circularly polarized light (lcp and rcp) ($\Delta\mathcal{A}_{l-r}$), with lcp being absorbed during $\Delta M_L=+1$ transitions and rcp being absorbed during $\Delta M_L=-1$ transitions. When a magnetic field is applied parallel to the axis of light propagation, there is a splitting of the orbitally degenerate 1E_u $\pi-\pi^*$ excited states into M_J+1 microstates and a first derivative-shaped Faraday \mathcal{A}_1 term is observed due to the Zeeman splitting of states. If a structural modification removes the main four-fold axis of symmetry so that there is a complete lifting of ground- and excited-state degeneracies, coupled oppositely signed and Gaussian-shaped Faraday \mathcal{B}_0 terms replace the derivative-shaped Faraday \mathcal{A}_1 terms, based on field-induced mixing of close-lying excited states linked by a magnetic dipole transition moment. When the $\Delta LUMO$ value is small relative to the bandwidths of the Gaussian-shaped \mathcal{B}_0 terms, a pseudo- \mathcal{A}_1 term is formed, which can be difficult to distinguish from an \mathcal{A}_1 term. Although free-base TPTPhenPs **5a-i** lack a four-fold axis of symmetry and are predicted to have deeply saddled structures (Figure 3), \mathcal{A}_1 terms are anticipated in the spectra of protonated dication species, since an S_4 axis of symmetry is retained.

Key information about the electronic structure can be derived from the sign sequences observed in the \mathcal{A}_1 terms or coupled oppositely signed \mathcal{B}_0 terms associated with the Q and B bands, since the $M_L=\pm 1$ property of the incident lcp and rcp photons must be conserved based on Newton's third

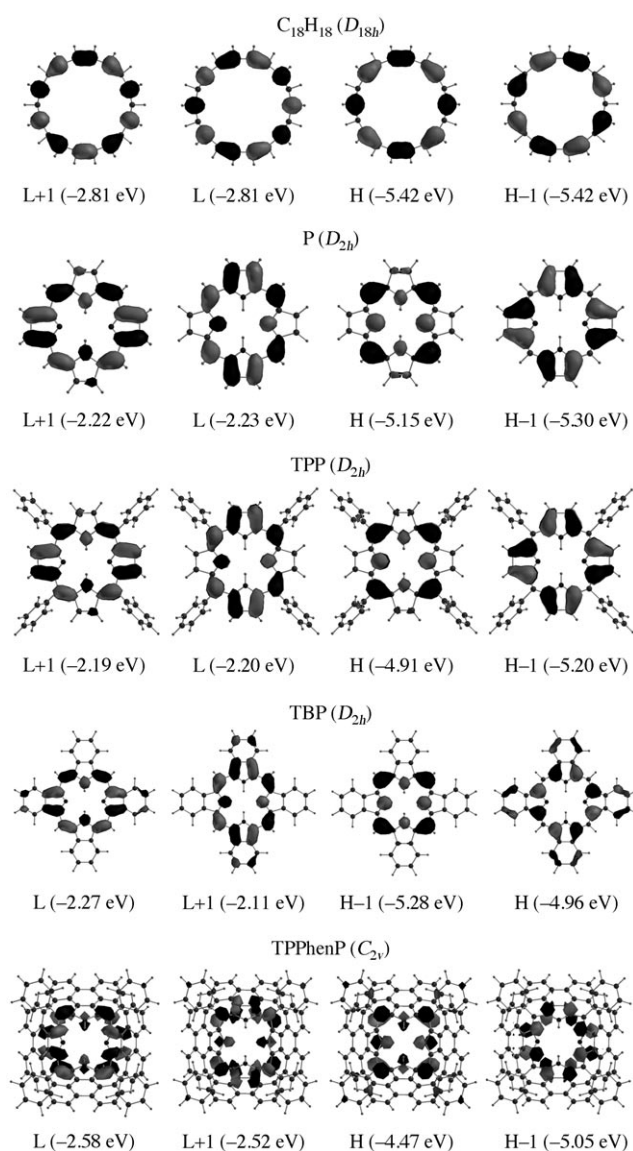


Figure 1. Frontier π MOs of a $C_{18}H_{18}$ parent hydrocarbon perimeter, porphyrin (P), tetraphenylporphyrin (TPP), tetrabenzoporphyrin (TBP), and tetraphenyltetraphenanthroporphyrin (TTPhenP, **5a**) at an isosurface value of 0.03 a.u. The same nodal patterns are consistently observed reflecting the $M_L = \pm 4, \pm 5$ properties of the four frontier π MOs of fused-ring-expanded porphyrinoids. Under the D_{2h} symmetry of P, the MOs from left to right are $1b_{3g}^*$, $1b_{2g}^*$, $1b_{1u}$, and $1a_u$, respectively.

law of motion.^[20,23] When an electron is electronically excited from the HOMO to the LUMO, the circular motion of the electron on the perimeter is no longer balanced by that of an electron in an MO of the opposing-handedness properties. Absorption of a photon by a cyclic π system, therefore, results in a circular redistribution of charge and hence to a magnetic moment aligned along the z axis perpendicular to the π system (Figure 2). The alignment of the magnetic moments with or against the applied field is determined by the OAM properties of the frontier π MOs derived from the HOMO and LUMO of the parent perimeter. When the OAM is greater in the LUMO level than in the HOMO

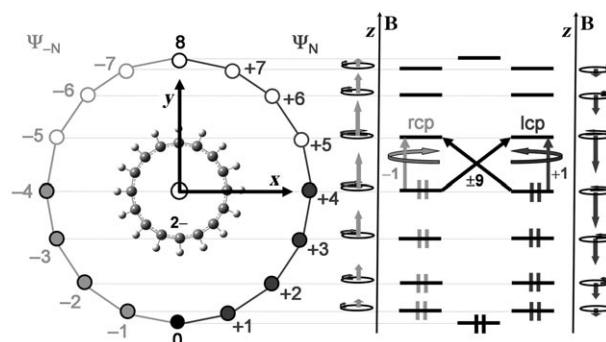


Figure 2. Left: Michl's perimeter model^[20] for $C_{16}H_{16}^{2-}$. The circle represents a diagrammatic representation of the clockwise and counterclockwise motion of π -system electrons on the inner ligand perimeter that generate the M_L value for each complex π MO. Center: The alignment and magnitude of the magnetic moments induced by the electron motion within each π MO can be predicted based on the right-hand rule and linear combination of atomic orbitals (LCAO) calculations. The moments aligned along the z axis with or against the applied field are shown diagrammatically.^[20] Right- and left-handedness is defined within classical optics looking towards the light source of the CD spectrometer (lcp and rcp = left and right circularly polarized light, respectively).

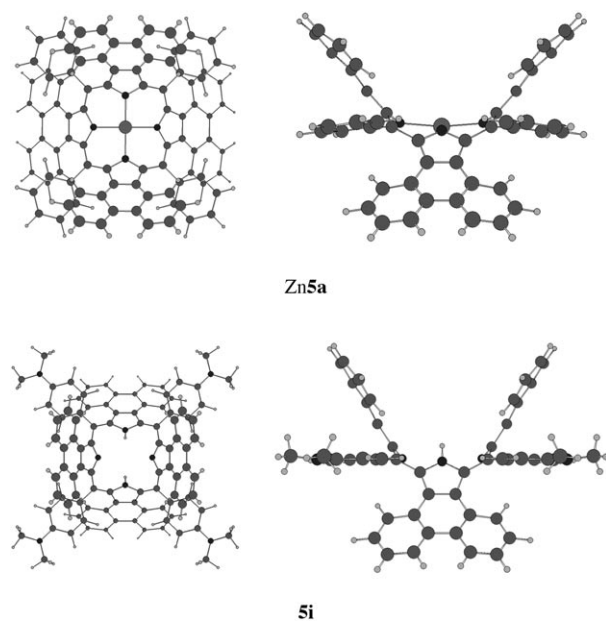


Figure 3. The B3LYP-optimized geometries of (top) **Zn5a** and (bottom) **5i** exhibit a deep saddled conformation when viewed along the (left) z and (right) y axes.

level, as is normally the case for most porphyrinoids, a negative particle is effectively formed on the perimeter, which circulates with the left- or right-handed motion of the incident photon. In contrast, when there is a marked quenching of the OAM of the LUMO level due to the introduction of a large Δ LUMO value by a structural perturbation, a positive particle circulates instead based on the hole left within the HOMO level. Application of Ampere's rule for solenoids can be used to demonstrate that when the LUMO level has greater OAM, a positive Faraday \mathcal{A}_1 term (i.e., a

negative/positive (+ve/−ve) sign sequence in ascending energy terms) is formed within the MCD spectrum, since the microstate associated with the absorption of rcp ($\Delta M_L = -1$) is stabilized as the induced magnetic moment is aligned with the applied field, whereas the microstate associated with the absorption of lcp ($\Delta M_L = +1$) is destabilized as the induced magnetic moment is aligned against the field.

Michl^[23] referred to cyclic polyenes in which $\Delta HOMO$, $\Delta LUMO \approx 0$ (such as TPTANPs) as soft MCD chromophores,^[19] since small structural modifications can potentially reverse the alignment of the induced magnetic moments of the π - π^* excited states and hence the sign sequence observed for the Faraday \mathcal{A}_1 terms or coupled oppositely signed Faraday \mathcal{B}_0 terms associated with the main Q_{00} and B_{00} bands. In the context of TPTANPs, metal complexes were found to exhibit anomalous negative Faraday \mathcal{A}_1 terms (i.e., a +ve/−ve sign sequence in ascending energy terms), whereas the normal −ve/+ve sign sequence was observed for free-base compounds and dication species.^[19] The unusual Faraday \mathcal{A}_1 terms in the MCD spectra of the metal complexes are believed to arise, because ligand saddling quenches the OAM properties of the LUMO level to a greater extent than those of the HOMO level. The availability of the more deeply saddled TPTPhenPs (Figure 3) provides additional insight into the effect of ligand saddling on the electronic structure and optical properties of porphyrinoids. Recent studies on core-modified tetrabenzoporphyrins^[27] and α -phenylated phthalocyanines^[28] have demonstrated that the results of DFT geometry optimizations are very similar to those obtained by X-ray crystallography when steric hindrance between peripheral fused rings results in severe ligand folding due to the lack of conformational flexibility. Trends observed in the experimental data for TPTPhenPs can, therefore, be readily compared to those predicted in theoretical calculations for B3LYP-optimized geometries, even in the absence of X-ray structures.

Results and Discussion

Synthesis of meso-tetraaryl tetraphenanthroporphyrins: A modified version of the Lindsey method^[29] was used to prepare a series of TPTPhenPs (**5a–i**) (Scheme 2). Phenanthro[9,10]pyrrole (**2**) is readily available based on a Barton–Zard reaction of 9-nitrophenanthrene (**1**) with ethyl isocyanacetate in the presence of the non-nucleophilic base 1,8-diazabicyclo[5.4.0]undec-7-ene (DBU).^[30] The ethyl ester group can be removed by heating **2** with potassium hydroxide in ethylene glycol at 170 °C to afford the tetracyclic compound **3** in excellent yield. A $BF_3 \cdot OEt_2$ -catalyzed condensation of **3** with benzaldehyde in dry CH_2Cl_2 at −50 °C for 3 h and subsequently at room temperature for 24 h generated a porphyrinogen (**4**), which was oxidized with 2,3-dichloro-5,6-dicyano-1,4-benzoquinone (DDQ) to afford the target porphyrin compound **5a** in 15% yield.^[22] A series of 4-substituted benzaldehydes (R = F, Cl, Br, I, Me, CN, NO_2 , NMe_2) were condensed with **3** as described above and porphyrins

5b–i were obtained in 10–19% yields. In contrast, porphyrins **5j** and **5k** could not be formed from 3-nitrobenzaldehyde and 2,5-dichlorobenzaldehyde under these conditions due to the increased steric hindrance associated with substituents at the *ortho* and *meta* positions. In contrast with the analogous TPTANP compounds, repeated attempts to synthesize the metal complexes of **5b–i** based on metal insertion reactions with metal salts also consistently failed.

Characterization of 5a–i: The compounds are all moderately to weakly soluble in most organic solvents with reddish-pink (e.g. **5a**, **5c**), greenish-blue (**5f**, **5h**), and blue (**5g**, **5i**) colors. The structures were characterized by MALDI-TOF MS, ¹H NMR spectroscopy, and elemental analysis (see the Experimental Section and Figures S1–S9 in the Supporting Information). For example, the MALDI-TOF mass spectrum of **5g** contains the anticipated molecular ion peak ($[M+H]^+$) at m/z 1315, and the ¹H NMR spectrum for **5g** in $CDCl_3$ in the presence of 1% deuterated trifluoroacetic acid (Figure 4) contains six peaks between $\delta = 6.8$ –8.9 ppm,

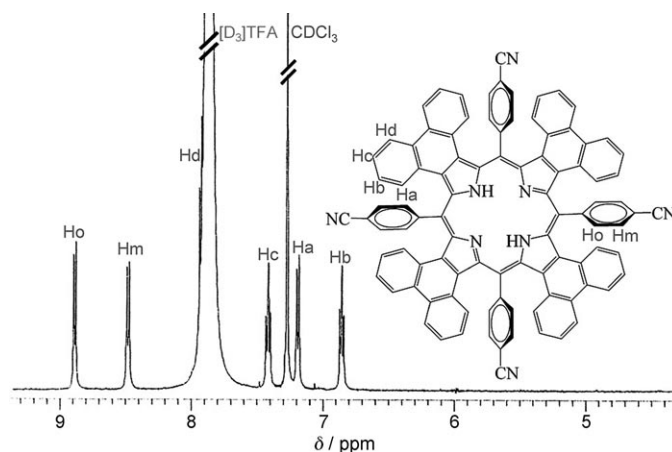


Figure 4. Partial 500 MHz ¹H NMR spectrum of **5g** in $CDCl_3$ containing 1% deuterated trifluoroacetic acid. The assignment of the proton signal is based on the integrated intensities and coupling patterns.

which is consistent with the anticipated symmetric aromatic structure. The phenanthrene protons closest to the meso-phenyl rings are shielded relative to those in TPhenP and can, therefore, be assigned to the upfield triplet at $\delta = 6.86$ ppm.^[31] The doublets at $\delta = 8.89$ and 8.48 ppm, respectively, can be assigned to the *ortho* and *meta* protons of the meso-phenyl rings, since they are deshielded by both the porphyrin macrocyclic and phenanthrene ring currents. The remaining protons lie in the typical aromatic range between $\delta = 7.0$ –7.5 ppm. These results for **5g**, and the broadly similar ¹H NMR spectra of **5a–f**, **5h**, and **5i** (Figures S1–S6, S8, and S9 in the Supporting Information), demonstrate that the structures of TPTPhenPs have reasonably high symmetry similar to those reported during recent studies on TPTANPs.^[16,18] The ¹H NMR spectra are consistent with the B3LYP geometry optimizations for **5a** and **5i**,^[32] which pre-

dict a deep saddlelike distorted conformation of the π system that results in a C_{2v} symmetry (Figure 3). Despite repeated efforts, single crystals suitable for X-ray crystallography could not be obtained. It should be noted that no X-ray structures have been reported for the similarly deeply saddled TPTANPs^[10,16,18,19] probably due to the impact of the severe ligand saddling on the π - π stacking properties in the solid phase.

Absorption, MCD, and fluorescence spectroscopy of free-base 5a-i: The optical spectra of **5a-i** in CHCl_3 are provided in Figures 5 and 6. Key data related to the major spectral bands are summarized in Table 1. The B bands are located at longer wavelengths than is observed for comparable

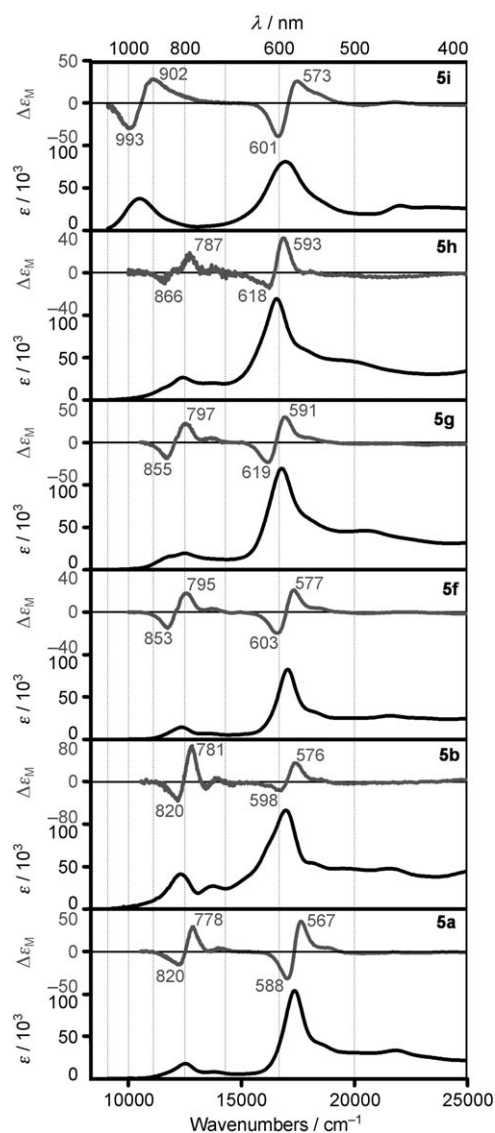


Figure 5. Absorption and MCD spectra of **5a**, **5b**, and **5f-i** recorded in 99:1 (v/v) CHCl_3 /ethanol at 298 K. The coupled pairs of overlapping Faraday \mathcal{B}_0 terms associated with the Q and B bands can be viewed as pseudo- \mathcal{A}_1 terms that arise from transitions into close-lying excited states that would be orbitally degenerate if a central metal were present.

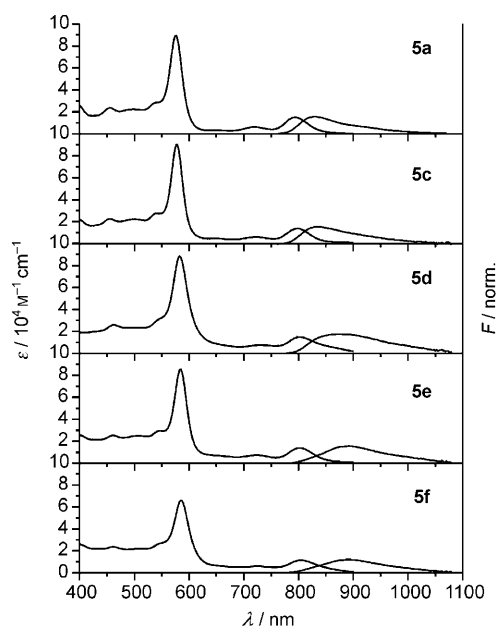


Figure 6. Absorption and fluorescence spectra of **5a** and **5c-f** in CHCl_3 at 298 K. The fluorescence bands are normalized on the lowest-energy absorption maxima.

Table 1. Absorption and fluorescence properties of **5a-i** in CHCl_3 at 298 K.

		B band		Q band		Fluorescence		
		λ_{abs} [nm]	$\log \epsilon$	λ_{abs} [nm]	$\log \epsilon$	λ_{em} [nm]	Φ_f [$\times 10^{-3}$]	τ_f [ns]
5a	-H	576	4.92	794	4.14	831	5.7	0.38
5b	$-\text{CH}_3$	584	4.97	803	4.31	851	5.2	0.32
5c	-F	576	4.96	794	4.14	833	6.0	0.41
5d	-Cl	582	4.95	805	4.17	870	3.9	0.25
5e	-Br	583	4.93	801	4.14	888	3.1	0.21
5f	-I	586	4.82	805	4.06	892	2.0	0.14
5g	-CN	596	4.98	798	4.14	907	2.3	0.19
5h	$-\text{NO}_2$	603	4.98	804	4.18	924	1.7	0.17
5i	$-\text{N}(\text{CH}_3)_2$	595	4.87	931	4.33	1004	1.2	0.14

TPTANP compounds (575–605 nm) and are redshifted by more than 150 nm relative to the parent *meso*-tetraphenylporphyrin (TPP) compound,^[10] although they retain high molar absorption coefficients of $\log \epsilon > 4.9$ despite the deep saddling of the ligand. The MO coefficients of the frontier π MOs are largely located on the inner ligand perimeter (Figure 1), so there is still considerable overlap between the MOs. Weaker Q_{00} and Q_{01} absorption bands are observed in the NIR region. The Q_{00} bands have comparable MCD intensity to the B bands due to the larger magnetic moments associated with the forbidden ($\Delta M_L = \pm 9$) transition. In contrast with most planar porphyrins^[26] and with TPTANPs,^[19] the absorption intensity of the Q_{00} bands is greater than that of the Q_{01} vibrational bands. This suggests that the Q_{00} bands become partially allowed due to a significant splitting of the MOs derived from the HOMO of the parent perimeter, and that vibrational borrowing from the allowed B band is therefore not the main intensity mechanism in the Q-band

region. The MCD intensity to the blue of the B band is very weak, since the MOs involved tend to be associated with the peripheral phenanthrene moieties rather than the inner perimeter of the π system. The OAM properties of the higher-energy excited states are, therefore, largely quenched by the ligand saddling. Across the entire **5a–i** series, a single intense set of oppositely signed \mathcal{B}_0 terms is observed for the Q_{00} and B bands of each spectrum with a $-ve/+ve/-ve/+ve$ sign sequence in ascending energy terms as has been reported previously for free-base TPTANP. This is the pattern anticipated when the $\Delta HOMO$ value is greater than the $\Delta LUMO$ value and the quenching of the OAM properties of the HOMO level of the parent perimeter is greater than that of the LUMO level.^[19,20]

In the series **5a**, **5c–f**, slight redshifts of 5–10 nm are observed for the B and Q_{00} bands, in an order consistent with the electron-withdrawing ability of the 4-halogeno substituent. In the near-infrared region (NIR), there are weak Q_{01} vibrational bands (≈ 720 nm) and more intense Q_{00} bands (≈ 800 nm) with around 5–10% and 15% of the intensity of the corresponding B bands, respectively. Substitution with strongly electron-withdrawing and -donating groups results in more pronounced changes to the TPTPhenP spectrum. In the presence of strongly electron-withdrawing $-\text{CN}$ (**5g**) and $-\text{NO}_2$ (**5h**) *para* substituents, there is a greater splitting of the *x*- and *y*-polarized Q_{00} bands, and the lower-energy Q_{00} band is observed as a broad shoulder between 850–970 nm. The B bands also shift markedly to 596 and 603 nm, respectively. The largest spectral changes are observed with strongly electron-donating $-\text{N}(\text{CH}_3)_2$ groups (**5i**). There is a marked redshift and intensification of the Q_{00} bands, whereas in contrast the B band lies at the same wavelength as that of **5b** and **5g** and is considerably broadened and lower in intensity.

All of the TPTPhenPs reported exhibit NIR fluorescence with quantum yields between 0.1 and 1.0% (Table 1). The fluorescence spectra generally form an approximate mirror image of the Q_{00} -band absorption spectra with maxima between 830 nm (**5a**, **5c**) and 1004 nm (**5i**), which represents an unprecedented wavelength for tetrapyrrole porphyrinoids. Stokes shifts of around 700 cm^{-1} are consistently observed.^[33] The fluorescence lifetimes are generally monoexponential and range between 0.14 and 0.41 ns for **5i** and **5c**, respectively. This suggests that the emissive state is rapidly quenched by intramolecular processes. The fluorescence quantum yield and lifetime data are of the same order of magnitude as those found for other highly distorted porphyrins such as dodecaphenylporphyrin^[34–36] (DPP): $\Phi_f = 2 \times 10^{-3}$, $\tau_f = 0.095$ ns in CHCl_3 .^[36] As is the case with DPP, the relatively low emissivity of these compounds can be ascribed to the high degree of nonplanarity,^[13] which facilitates intersystem crossing and internal conversion, and the growing influence of internal conversion as a function of the shift of the emission band into the NIR region due to the energy-gap rule.^[37] The increase in the rate constant of nonradiative deactivation^[38] observed for the 4-halogeno compounds, 2.4 (**5c**) < 3.9 (**5d**) < 4.7 (**5e**) $< 7.0 \times 10^9\text{ s}^{-1}$ (**5f**), is consistent

with an internal heavy-atom effect that has been reported previously for porphyrins.^[39–42] Phosphorescence could not be detected for any of the dyes probably due either to the limited detection range (≤ 1100 nm) of the instrument employed or to the weakness of such luminescence due to the marked redshift of the lowest-energy absorption band.

Absorption and fluorescence spectroscopy of $5aH_2^{2+}$ – $5hH_2^{2+}$: Compound **5i** possesses four peripheral sites at the $-\text{N}(\text{CH}_3)_2$ groups that are susceptible to protonation and can, therefore, be readily transformed from being strongly electron-donating to strongly electron-withdrawing. Before discussing **5i** in detail, it is important to first understand the spectral changes that occur when the inner perimeters of the π systems of **5a–5h** are protonated to form conventional dication species. Data were obtained in the presence of 1% trifluoroacetic acid (TFA) so that only doubly protonated species are present in solution (Table 2 and Figure 7). The B

Table 2. Absorption and fluorescence properties of protonated species of **5a–i** in CHCl_3 at 298 K.

		B band		Q band		Fluorescence	
		λ_{abs} [nm]	$\log \epsilon$	λ_{abs} [nm]	$\log \epsilon$	λ_{em} [nm]	Φ_f [$\times 10^{-3}$]
5aH₂²⁺	–H	579	5.04	803	4.21	838	8.0
5bH₂²⁺	–CH ₃	587	5.01	816	4.34	858	10.0
5cH₂²⁺	–F	579	5.06	804	4.25	837	10.1
5dH₂²⁺	–Cl	584	5.04	807	4.32	842	6.8
5eH₂²⁺	–Br	586	5.02	808	4.33	844	6.5
5fH₂²⁺	–I	589	4.99	811	4.29	851	3.9
5gH₂²⁺	–CN	596	5.18	803	4.28	834	4.1
5hH₂²⁺	–NO ₂	602	5.11	806	4.38	839	4.4
5iH₃³⁺	–N(CH ₃) ₂	636	4.70	1015	4.55	n.d. ^[a]	–
5iH₆⁶⁺	–N(CH ₃) ₂	580	n.d. ^[b]	784	n.d. ^[b]	810	(4.0) ^[b]

[a] No fluorescence could be detected since the detection system could only be employed up to 1100 nm. [b] Could not be reliably determined.

bands of **5aH₂²⁺**–**5fH₂²⁺** shift slightly to the red by around 3 nm while gaining markedly in intensity. No redshifts are observed for **5gH₂²⁺** and **5hH₂²⁺**. Similar trends are observed in the Q bands of TPTPhenPs with weakly electron-donating or -accepting *para* substituents. Redshifts of 7–15 nm and moderate intensity increases are observed in the spectra of **5aH₂²⁺**–**5fH₂²⁺**. The Q bands of **5gH₂²⁺** and **5hH₂²⁺** narrow significantly and, in contrast with the free-base spectra, display features very similar to those of **5aH₂²⁺**–**5fH₂²⁺** (Figures 5 and 7). Despite the marked differences in the electron-withdrawing and -donating properties of the *para* substituents, the absorption and MCD spectra of **5aH₂²⁺**, **5fH₂²⁺**, **5gH₂²⁺** and **5iH₆⁶⁺** are almost identical, in marked contrast with the corresponding free-base spectra. Positive Faraday \mathcal{A}_1 terms are consistently observed for the Q_{00} , Q_{01} , and B_{00} bands. The changes in the fluorescence spectra closely reflect those observed in the absorption spectra. Virtually identical emission bands are observed for **5aH₂²⁺**–**5hH₂²⁺** at (846 ± 12) nm with Stokes shifts of $(530 \pm 70)\text{ cm}^{-1}$. The fluorescence quantum yields are between 150–250% higher than those of the corresponding

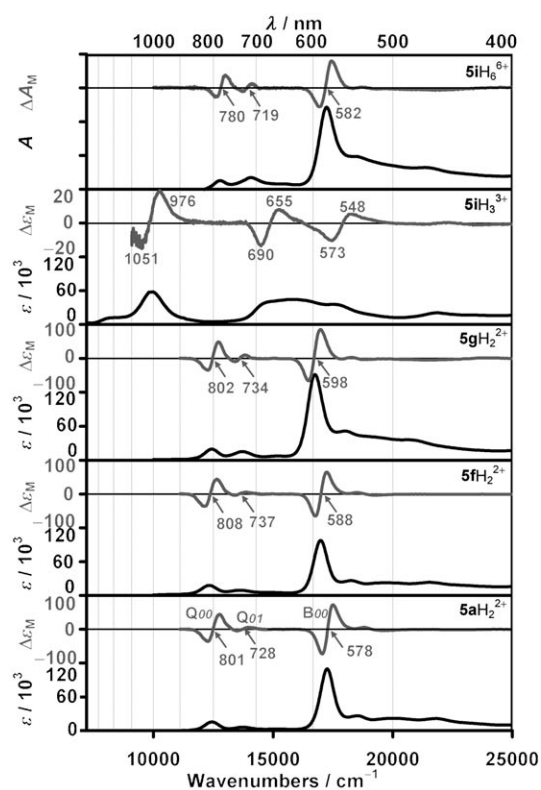


Figure 7. Absorption and MCD spectra of $5aH_2^{2+}$, $5fH_2^{2+}$, and $5gH_2^{2+}$ recorded in 99:1 (v/v) $CHCl_3$ /ethanol that contained 1% of TFA; $5iH_3^{3+}$ obtained during a titration of a solution of $5i$ in 99:1 (v/v) $CHCl_3$ /ethanol after the addition of 50 equiv of TFA; and $5iH_6^{6+}$ recorded in pure TFA. The close correspondence between the absorption band maxima and the zero point of the first-derivative-shaped MCD band is consistent with the presence of three Faraday \mathcal{A}_1 terms that arise from x/y -polarized Q_{00} , Q_{01} , and B_{00} bands.

free bases, as has been reported previously for other highly sterically hindered porphyrins such as DPP ($DPPH_2^{2+}$: $\Phi_1 = 7 \times 10^{-3}$, $\tau_f = 0.33$ ns in $CHCl_3$).^[36]

The B3LYP geometry optimization for $5iH_2^{2+}$ (Table 3) predicts that the electrostatic repulsion introduced by the two additional protons on the inner ligand perimeter leads to a further deepening of the saddled structure. Similar effects have previously been reported for tetraphenylporphyrinoids with the *meso*-phenyl rings tilting into the plane of the inner perimeter of the π system.^[43,44] A marked intensification of the Q-band region has been reported on this basis for $DPPH_2^{2+}$.^[45] A destabilization of the HOMO, which has large MO coefficients on the four pyrrole nitrogen atoms (Figure 1), leads to an increase in the $\Delta HOMO$ value from 0.85 to 1.12 eV on going from $5i$ to $5iH_2^{2+}$ and hence to the increase in the molar absorption coefficients that is observed for the Q_{00} bands of $5aH_2^{2+}$ and $5cH_2^{2+}$ - $5fH_2^{2+}$, since there is a mixing of the allowed and forbidden properties of the Q and B bands. An increased $\Delta HOMO$ value also accounts for the positive \mathcal{A}_1 terms that are observed for the Q_{00} and B bands of TPTPhen H_2^{2+} species. The quenching of the OAM properties of the HOMO level on this basis can be expected to outweigh the saddling-related quenching of the

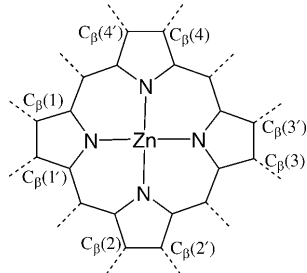
LUMO level that is believed to cause the anomalous negative \mathcal{A}_1 terms observed in the MCD spectra of TPTANP metal complexes.^[19]

Absorption, MCD, and fluorescence spectroscopy of the protonated species of $5i$ and theoretical calculations:

Titration were carried out for the protonation of $5i$ in the presence of TFA (Figure 8). Up to six protons can be added, since the four $-N(CH_3)_2$ groups are susceptible to protonation. Complete protonation to form the $5iH_6^{6+}$ was achieved in a 99:1 $CHCl_3$ /ethanol solvent mixture. DFT geometry optimizations and TD-DFT calculations of TPTPhenPs are expensive in terms of machine time, so they have only been carried out for $5a$, $5i$, and $5iH_2^{2+}$. Additional calculations were carried out on the corresponding TPP model complex with no peripheral phenanthrene rings, *meso*-tetrakis(4-*N,N*-dimethylaminophenyl)porphyrin ($6i$) (Figure 9; for chemical structure, see Scheme 1). The spectra of free-base $5i$ and of the protonated species are expected to be broadly similar to those of $6i$ since the absorption spectrum of $5a$ is very similar to that of TPP with the exception of the marked redshift of the Q and B bands. The additional information provided by MCD spectroscopy can be used to identify the spectra of each protonated species during the titration of $5i$. Since there is no three-fold or higher axis of symmetry and hence no orbitally degenerate excited states, coupled oppositely signed and Gaussian-shaped x - and y -polarized \mathcal{B}_0 terms are anticipated in the MCD spectra of $5i$, $5iH_3^{3+}$, $5iH_4^{4+}_{adj}$, $5iH_4^{4+}_{opp}$, and $5iH_5^{5+}$, whereas x/y -polarized and first-derivative shaped \mathcal{A}_1 terms are anticipated in the spectra of $5iH_2^{2+}$ and $5iH_6^{6+}$ due to the presence of an S_4 axis of symmetry (Figure 8).^[46] The visible and near-IR regions of the calculated spectra of $5i$ and $5iH_6^{6+}$ are dominated by the Q and B bands. TD-DFT and ZINDO/s calculations predict the presence of additional coupled and oppositely signed \mathcal{B}_0 terms or \mathcal{A}_1 terms in the spectra of $5iH_2^{2+}$, $5iH_3^{3+}$, $5iH_4^{4+}_{adj}$, $5iH_4^{4+}_{opp}$, and $5iH_5^{5+}$ based on configurational interaction between the Q and B excited states and states associated with two *meso*-aryl substituent MOs, which have the same symmetry properties as the MOs that arise from the HOMO of the parent perimeter (Figures 9 and 10; and Figures S10–S12 in the Supporting Information). These MOs are markedly destabilized upon partial protonation of the peripheral $-N(CH_3)_2$ groups (Figure 10).

The most striking features of the initial stages of the titration spectra are the intense band centered at around 1000 nm and a weaker, extremely redshifted band between 1150–1300 nm region (Figure 8). These bands can be assigned as Q_{00} bands, since a marked destabilization of the HOMO of $6i$ is predicted upon protonation (Figure 10 and Figure S12 in the Supporting Information). The energy of the other MO that arises from the doubly degenerate HOMO of the parent perimeter (i.e., the $1a_u$ MO of P) remains relatively constant due to the lack of significant MO coefficients on the pyrrole nitrogen atoms (Figure 10). Since there is a close correspondence between band centers in the absorption and MCD spectra after the addition of 20 equiv

Table 3. Distances [Å] between the carbon atoms of the bonds that define the β positions of opposite pyrroles (see structure for atom numbering) of **Zn5a** and a series of free-base porphyrinoid compounds and Zn^{II} complexes based on B3LYP geometry optimizations with 6-31G(d) basis sets, the average HOMO–LUMO bandgap (H–L) [eV], the observed Q- and B-band (Q^{obs} and B^{obs}) wavelengths [nm], solvent used, and references.



	Carbon atoms				H–L	Q^{obs}	B^{obs}	Solvent ^[a]	Ref.
	1–3	1'–3'	2–4	2'–4'					
5iH₂²⁺	6.64	6.64	6.64	6.64	–	–	–	–	
5i	6.79	6.79	6.74	6.74	4.31	993, 902 ^[c]	601, 573 ^[c]	CHCl_3	
5a	6.90	6.90	6.87	6.87	4.36	809, 776 ^[c]	586, 568 ^[c]	CHCl_3	
Zn5a	7.27	7.26	7.27	7.27	4.43	–	–	–	
ZnTPhenP	8.40	8.41	8.40	8.41	4.77	668 ^[d]	482 ^[d]	CHCl_3	[29]
TPTANP	7.84	7.84	8.07	7.99	4.94	776, 750 ^[c]	575, 558 ^[c]	THF	[19]
ZnTPTANP	8.07	8.07	8.07	8.07	4.42	717 ^[c]	563 ^[c]	CH_2Cl_2	[19]
ZnTANP ^[b]	8.62	8.62	8.62	8.62	4.63	702 ^[d]	528 ^[d]	CHCl_3	[17]
ZnTPNP	8.18	8.18	8.18	8.18	4.65	710	470	CHCl_3	[49a]
ZnNP ^[b]	8.55	8.55	8.55	8.55	4.83	701	439	DMF	[49b]
TPTBP	8.30	8.30	8.32	8.32	4.68	670, 640 ^[c]	472, 456 ^[c]	CHCl_3	[49d]
ZnTPTBP	8.27	8.27	8.27	8.27	4.78	651 ^[c]	459 ^[c]	CHCl_3	[49d]
TBP ^[b]	8.69	8.69	8.70	8.70	4.89	663, 614 ^[c]	435, 418 ^[c]	CHCl_3	[27]
ZnTBP ^[b]	8.65	8.65	8.85	8.65	4.97	628	433	DMF	[14]
ZnDPP	8.07	8.07	8.05	8.05	4.78	639	463	<i>o</i> -DCB	[49c]
6i	8.52	8.52	8.54	8.54	4.89	634 ^[d]	447 ^[d]	CH_2Cl_2	[45]
TPP ^[b]	8.64	8.64	8.61	8.61	4.97	641, 544 ^[c]	422, 413 ^[c]	DMA	[19]
ZnTPP ^[b]	8.60	8.60	8.60	8.60	4.97	586 ^[c]	419 ^[c]	CH_2Cl_2	[19]
P ^[b]	8.62	8.62	8.63	8.63	5.12	618, 525 ^[e]	412, 397 ^[e]	DMA	[19]
ZnP ^[b]	8.60	8.60	8.60	8.60	5.20	561	401	C_6H_6	[21]

[a] THF, DMF, *o*-DCB, and DMA refer to tetrahydrofuran, dimethylformamide, *o*-dichlorobenzene, and dimethylacetamide, respectively. [b] Planar Zn^{II} complexes with D_{4h} symmetry and free-base compounds with D_{2h} symmetry have values between 8.50 and 8.70 Å. [c] Data derived from MCD spectroscopy. [d] Absorption-band values are for dication species generated in the presence of 1% TFA rather than for Zn^{II} complexes. [e] Data derived from a MCD spectrum of free-base octaethylporphyrin, since comparatively little research has been carried out on the parent unsubstituted porphyrin.

of TFA rather than with the zero points of first-derivative-shaped signals as is typically observed with \mathcal{A}_1 terms (Figure 7), it is safe to conclude that the spectrum is dominated by well-resolved Faraday \mathcal{B}_0 terms, and can, therefore, be assigned to the 5iH_3^{3+} species rather than to the 5iH_2^{2+} dication. Only slight changes are observed in the absorption spectrum at low acid concentrations, thus making it difficult to trace the initial protonation of the two core pyrrolic nitrogen atoms. Similar results were reported by Walter et al. during the titration of the **6i** model compound.^[17,48] Full protonation to form 5iH_6^{6+} can be readily achieved when the compound is dissolved in concentrated TFA and results in a “normal” 5H_2^{2+} spectrum (Figure 7) with an intense and narrow B band at 580 nm and well-resolved Q_{01} and Q_{00} bands at 710 and 784 nm, since the electron-donating properties of all of the $-\text{N}(\text{CH}_3)_2$ groups are eliminated. The Faraday \mathcal{A}_1 terms associated with these 5iH_6^{6+} bands can be readily identified in the latter stages of TFA titrations of **5i** (Figure S11). With the exception of 5iH_6^{6+} , fluorescence

spectra could not be measured for the various protonated species due to their strongly red-shifted absorption bands.

Influence of annelation on conformation and band positions:

The optical spectroscopy of radially symmetric porphyrinoids can be readily accounted for based on the influence of different structural perturbations on the energies of the four frontier π MOs with $M_L = \pm 4, \pm 5$ nodal properties that arise from the HOMO and LUMO of the parent perimeter (Figure 11, Tables 3 and 4; and Figure S13 in the Supporting Information). With the exception of a slight lifting of the orbital degeneracy of the $1e_g^*$ LUMO due to the loss of the fourfold axis of symmetry, the energies of the MOs of the free-base compounds are broadly similar to those of the corresponding Zn^{II} complexes. The closed-shell d^{10} configuration of Zn^{II} makes Zn^{II} –porphyrinoids ideal model complexes for studying how trends in the energies of the four frontier π MOs affect the wavelengths of the Q and B bands. Fused-ring expansion with benzene rings destabilizes the $1a_u$ MO, which has large MO coefficients on the β -carbon atoms of the pyrrole moieties.

This leads to a significant decrease in the first oxidation potential reported for TBP and ZnTBP relative to P and ZnP, Table 5), since it is easier to remove an electron from the HOMO. A marked redshift and intensification of the Q band is observed upon going from ZnP to ZnTBP to ZnTNP due to the lower average HOMO–LUMO bandgap and larger ΔHOMO value (Figure 11 and Table 4).^[19] An average bandgap is calculated because when real rather than complex MOs are considered, the Q and B bands of porphyrins arise from close to equal contributions of one-electron transitions from the two occupied MOs derived from the parent perimeter HOMO to the two unoccupied MOs derived from the parent perimeter LUMO (Table 4).^[19,27]

The introduction of phenyl groups to form ZnTPP, ZnTPTBP, and ZnTPTNP destabilizes the $1b_{1u}$ MO due to the large MO coefficients at the *meso*-carbon atoms, thereby resulting in a further decrease in the average HOMO–

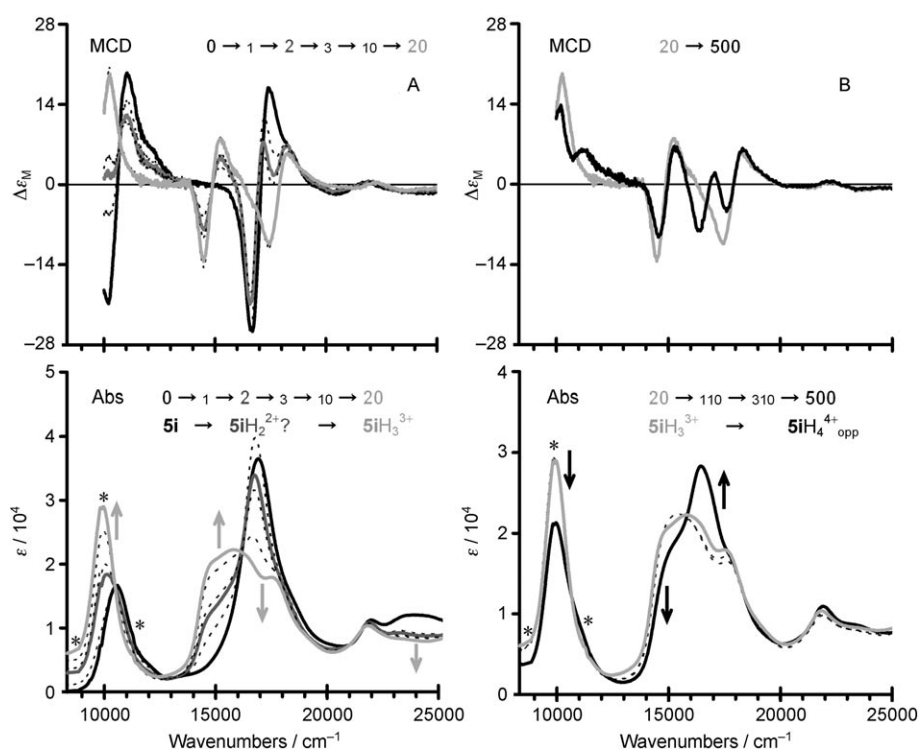


Figure 8. Absorption and MCD titration spectra of **5i** (14 μM) with TFA in a 99:1 CHCl_3 /ethanol solvent mixture. The molar equivalents of TFA added and the assignment of spectra to species 5iH_2^{2+} , 5iH_3^{3+} , and $5\text{iH}_4^{4+}_{\text{opp}}$ are indicated. Asterisks denote narrow regions of the absorption spectra in which the data sets are potentially slightly problematic due to the subtraction of strong solvent bands. Later stages of the titration are included as Supporting Information. A consistent set of isosbestic points is not observed between 0–20 equiv TFA (A), so an intermediate species is probably present, which is speculatively assigned as 5iH_2^{2+} . The MCD spectrum at 20 equiv is dominated by Faraday \mathcal{B}_0 terms, since the MCD and absorption band maxima correspond with each other, and can therefore be assigned to 5iH_3^{3+} , since first-derivative-shaped \mathcal{A}_1 terms would be anticipated for 5iH_2^{2+} . The spectrum of the next protonated species is observed at 500 equiv (B), which is assigned tentatively to $5\text{iH}_4^{4+}_{\text{opp}}$ instead of $5\text{iH}_4^{4+}_{\text{adj}}$ on the basis of the similarity of predicted NIR-band energies for 6iH_3^{3+} and $6\text{iH}_4^{4+}_{\text{opp}}$ (Figure 9).^[46] Isosbestic points are not observed on subsequent additions of TFA (Figure S11 in the Supporting Information) due to partial ring decomposition, but the spectra of 5iH_5^{5+} and 5iH_6^{6+} can be readily identified.

LUMO bandgap and redshifts of the Q and B bands. Additional marked redshifts are observed in the spectrum of ZnDPP relative to that of ZnTPP due to the effect of steric hindrance at the ligand periphery on the four frontier π MOs (Table 3), which is predicted by B3LYP geometry optimizations to result in a marked saddling distortion of the π system. The decrease in the average HOMO–LUMO bandgap predicted for ZnDPP is associated primarily, but not exclusively, with a destabilization of the $1b_{1u}$ MO (Figure 11 and Table 3). This results in a marked decrease in the first oxidation potential reported for ZnDPP relative to ZnTPP (Table 5). As was demonstrated in a recent study of nonplanar phthalocyanines with peripheral phenyl substituents,^[28] trends in the gap between the first oxidation and reduction potentials ($\Delta E_{\text{ox-r}}$) mirror those observed in the HOMO–LUMO bandgap and in the observed and calculated Q-band energies, since the first oxidation and reduction potentials vary with the energies of the HOMO and LUMO. The agreement is not expected to be exact, however, since the Q-band energies are related to the energies of all four fron-

tier π MOs derived from the HOMO and LUMO of the parent perimeter, whereas the redox properties are determined by the energies of the HOMO and LUMO.

In contrast with what is observed upon fused-ring expansion with benzene rings, there is only a minor destabilization of the $1a_u$ MO when acenaphthalene and phenanthrene moieties are added to the porphyrin π system. A stabilization of the LUMO results in a narrowing of the average HOMO–LUMO bandgap, however, and a marked redshift of the Q and B bands of ZnTPhenP and ZnTPTANP relative to ZnTBP. Although the average HOMO–LUMO bandgap of ZnTPhenP is predicted to be larger than that of ZnTANP, slightly greater redshifts are predicted for the Q and B bands of TPTPhenP and ZnTPTPhenP relative to those of TPTANP and ZnTPTANP due to a marked destabilization of the $1b_{1u}$ MO caused by the greater saddling of the ligand (Table 3), which rotates the *meso*-phenyl rings into the plane of the π system (Figure 3). The decreases anticipated in the first oxidation and reduction potentials of

5i and **6i** relative to **5a** and TPP, respectively, upon substitution with $-\text{N}(\text{CH}_3)_2$ groups based on the redshift of the Q bands and the narrowing of the calculated HOMO–LUMO bandgaps (Figures 5 and 9–11), are observed (Table 5), since it is easier to add an electron when the LUMO is stabilized and to remove an electron when the HOMO is destabilized.

Although there is a relatively small redshift of the B bands of TPTPhenP (568 and 586 nm) relative to TPTANP (558 and 575 nm),^[19] the B and Q bands of ZnTPhenP (482 and 668 nm) are predicted to lie well to the blue of those of ZnTANP (528 and 702 nm) (Figure 11). Similarly, the electronic absorption spectrum of TPTANPH₂²⁺ contains B and Q₀₀ bands at 565 and 760 nm, respectively,^[16] whereas the corresponding bands for **5aH**₂²⁺ are centered only slightly to the red at 579 and 803 nm, and the Q and B bands of TANPH₂²⁺ (702 and 528 nm)^[17] lie well to the red of those of TPhenPH₂²⁺ (668 and 482 nm).^[17] The significantly deeper saddling (Table 3), therefore, appears to be the main cause of the redshift of the Q and B bands of the TPTPhenP ligand relative to those of TPTANP, rather than the incorpo-

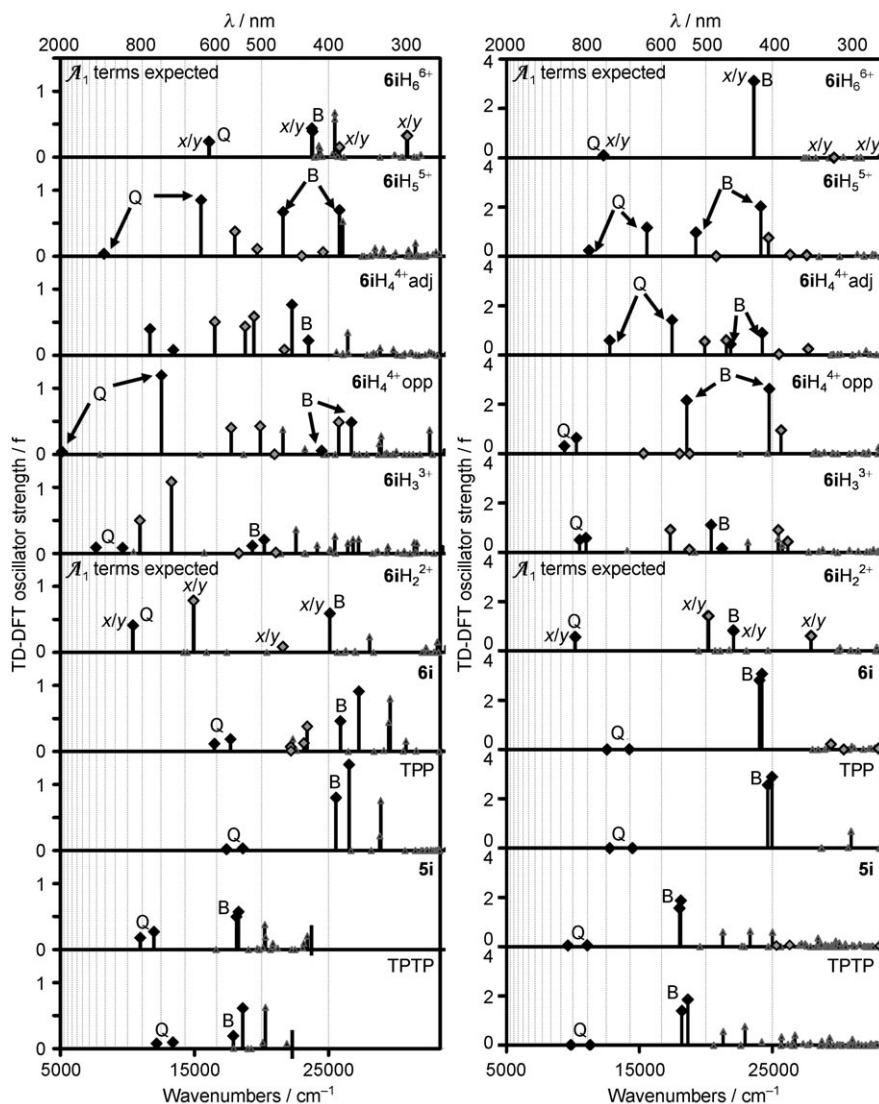


Figure 9. Left: The TD-DFT- and (right) ZINDO/s-calculated electronic absorption spectra of **5a**, **5i**, TPP, **6i**, **6iH₂²⁺**, **6iH₃³⁺**, **6iH₄⁴⁺adj**, **6iH₄⁴⁺opp**, **6iH₅⁵⁺**, and **6iH₆⁶⁺**. Transitions associated primarily with the four frontier π MOs from Gouterman's 4-orbital model,^[21] and two additional MOs with the same symmetry properties as the HOMO and HOMO-1 of P located primarily on the phenyl substituents (Figure 11), which are responsible for the additional charge-transfer bands of protonated species, are indicated with large black and light-gray diamonds, respectively. Details of the most intense bands of the ZINDO/s calculations are provided as Supporting Information. The TD-DFT calculations predict multiple sets of intense *x*- and *y*-polarized bands in the B-band regions of the TPP and **6a** spectra, whereas only one intense set of bands is observed experimentally as predicted in the ZINDO/s calculations (Figure 7). Similar issues have recently been reported with other porphyrinoid TD-DFT calculations.^[19,27]

ration of the phenanthrene moieties. The marked increase in the Δ HOMO value due to a destabilization of the $1b_{1u}$ MO (Figure 1 and Figure 12) leads to an intensification of the Q-band region of **5i** relative to that of **5a**.^[20] The larger Δ HOMO values predicted in TPTPhenP calculations relative to those of the corresponding TPTANPs coupled with the relatively small Δ LUMO values (Figure 12) accounts for the absence of the anomalous MCD band sign sequences observed in the MCD spectra of metal TPTANP complexes,^[19] since the OAM of the incident photon is conserved by the circulation of negative charge in the LUMO

level as is normally the case with radially symmetric porphyrinoids. Although attempts to form metal complexes of TPTPhenPs have proven unsuccessful, it is worth noting that the calculated Q- and B-band wavelengths for Zn**5a** also lie slightly to the red of those predicted for ZnTPTANP, despite the fact that the corresponding bands for ZnTPhenP lie well to the blue of those of ZnTANP (Figure 11). A slightly shallower saddling is predicted for Zn**5a** relative to the free-base compound and dication species (Table 3). In contrast, although a saddling of the ligand is predicted for ZnTPTANP, the B3LYP-optimized structure of TPTANP contains markedly different levels of ligand folding along the *x* and *y* axes with the *x*-axis acenaphthalene moieties tilted slightly out of a parallel alignment (Table 3). The apparent loss of structural flexibility when phenanthrenes replace the acenaphthalene moieties suggests that the steric crowding at the periphery of the TPTPhenP ligand results in a degree of saddling that is too deep and too rigid for a metal to be readily incorporated into the central cavity. It should be noted that the ZINDO/s calculation for free-base TPTANP does not provide an accurate prediction of the wavelengths of the Q and B bands (Figure 11), whereas the wavelengths predicted by TD-DFT for the same B3LYP-optimized structure are consistent with the

trends observed in the experimental and calculated data (see the Supporting Information).

Influence of the electronic nature of the meso substituents on band positions: TD-DFT and ZINDO/s calculations predict that the introduction of electron donating $-\text{N}(\text{CH}_3)_2$ groups at the *para* positions of the phenyl groups to form **5i** and **6i** destabilizes the four frontier π MOs (Figure 11 and Figure S13 in the Supporting Information). The introduction of substituents on the phenyl group provides scope for fine-tuning the properties of TPTPhenPs based on the Hammett

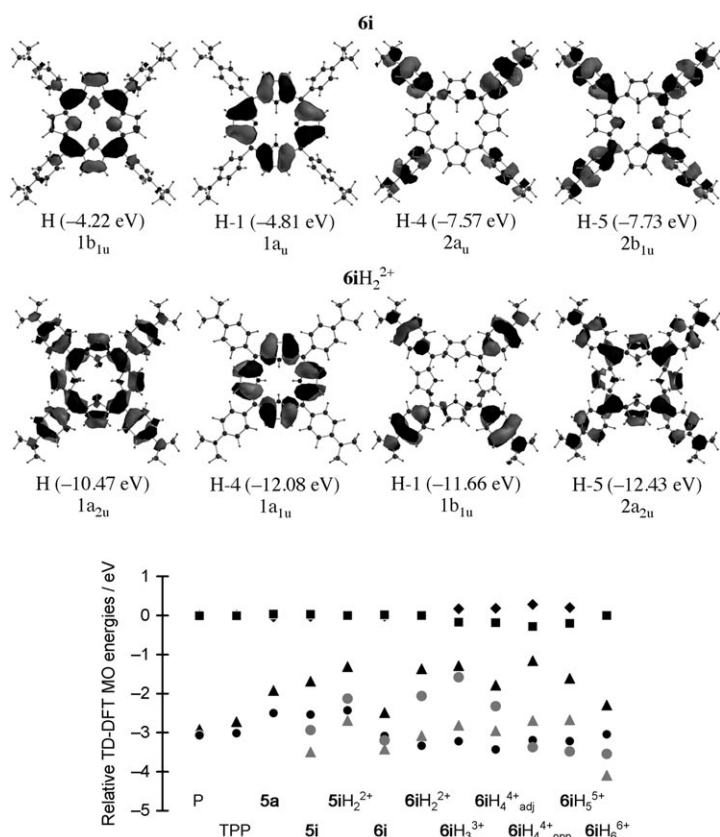


Figure 10. Top: The nodal patterns of the four key frontier π HOMOs of **6i** and **6iH₂²⁺** at an isosurface of 0.02 a.u. based on a B3LYP geometry-optimized structure derived using 6-31G basis sets. The axes are aligned so that the x and y axes lie horizontal and vertical in the plane of the page, respectively. H and H- n denote the HOMO and the n th MO in descending energy from the HOMO, respectively. Bottom: Trends in the relative energies [eV] of the key frontier π MOs of **P**, TPP, **5a**, **5i**, **5iH₂²⁺**, **6i**, **6iH₂²⁺**, **6iH₃³⁺**, **6iH₄^{4+adj}**, **6iH₄^{4+opp}**, **6iH₅⁵⁺**, and **6iH₆⁶⁺** relative to the average energy of the two MOs associated with the LUMO of the parent perimeter (i.e., $1b_{2g}^*$ and $1b_{3g}^*$ in the case of **P**; Figure 1). Black circles, triangles, squares, and diamonds denote MOs derived from the $1a_u$, $1b_{1u}$, $1b_{2g}^*$, and $1b_{3g}^*$ MOs of **P**, respectively (Figure 1 and Figure S10 in the Supporting Information), which are the four frontier π MOs that form the basis of Gouterman's 4-orbital model.^[21] Light-gray triangles and circles denote additional MOs introduced by the peripheral $-N(CH_3)_2$ groups with b_{1u} and a_u symmetry (under the D_{2h} symmetry of **P**), respectively (Figure 10, top), which play a key role in additional charge-transfer bands calculated to lie at similar energies to the Q and B bands in the spectra of **6iH₂²⁺**, **6iH₃³⁺**, **6iH₄^{4+adj}**, **6iH₄^{4+opp}**, and **6iH₅⁵⁺**. The corresponding plot of the ZINDO/s MO energies is provided in Figure S12 in the Supporting Information.

parameter (σ_p). It has long been known that linear plots can be obtained for $E_{1/2}$ versus $4\sigma_p$ for the first and second reduction and oxidation potentials of structurally related tetraphenylporphyrins.^[51] For example, in the mid-1970s, Kadish and Morrison^[52] reported linear trends in the redox values of free-base (p -X)TPP compounds with $-OCH_3$, $-CH_3$, $-H$, $-F$, $-COOCH_3$, $-Cl$, $-CN$, and $-NO_2$ substituents. The deep saddling distortion of the π system of (p -X)TPTPhenPs predicted in the B3LYP geometry optimizations of **5a** and **5i** (Figure 3 and Table 3) tilts the *meso*-phenyl rings almost into the plane of the four pyrrole nitrogen atoms, thereby

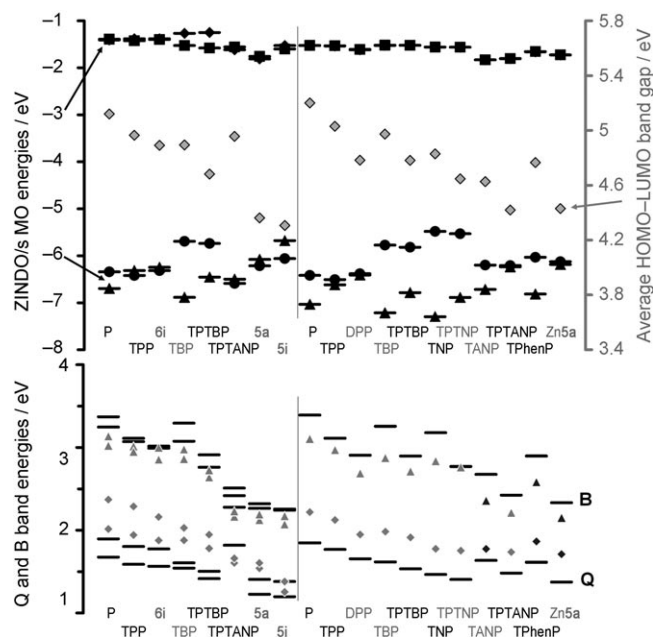


Figure 11. Top: ZINDO/s MO energies of a series of the free-base compounds and zinc complexes of porphyrinoids based on a set of B3LYP geometry optimizations with 6-31G(d) basis sets. Black circles, triangles, diamonds, and squares denote the $1a_u$, $1b_{1u}$, $1b_{2g}^*$, and $1b_{3g}^*$ frontier π MOs of **P**, respectively, and the MOs of the other compounds that exhibit the same $M_L = \pm 4, \pm 5$ nodal patterns. Gray diamonds denote the average HOMO-LUMO bandgap taking into account all four MOs associated with the HOMO and LUMO of the parent perimeter. Bottom: Experimental and calculated Q- and B-band energies are denoted with gray diamonds and triangles and black lines, respectively.^[10b,17,19,21,27,31,48,49] Black diamonds and triangles denote values derived from dication species rather than the Zn^{II} complexes of TANP, TPhenP, and **5a**.^[17,31] The corresponding plot for the TD-DFT calculations is provided in Figure S13 in the Supporting Information.

facilitating conjugation between the *meso* groups and the inner perimeter of the π system. As a result, even subtle electronic effects like those that arise from the halogen substituent series, **5c-f**, alter the optical spectroscopy to a readily observable extent (Figure 6 and Table 6). For example, in the case of electron-withdrawing substituents, a plot of the B-band maxima versus $4\sigma_p$ yields a strong correlation for **5c-e**, **5g**, and **5h** (Figure 13). A change in the aryl substituent can be expected to modify the energies of the Q and B bands based on changes in the ΔE_{o-r} value and the magnitude of the HOMO-LUMO bandgap. This is more difficult to follow in the Q-band region in which much of the absorption band intensity is vibrational rather than electronic in origin and there is often a marked splitting of the Q_x and Q_y bands.

When there is limited configurational interaction between the S1 state and higher $\pi-\pi^*$ energy excited states, trends in the energy of the lowest-energy $\pi \rightarrow \pi^*$ band will mirror those observed in the HOMO-LUMO bandgap and ΔE_{o-r} values. In the context of porphyrinoids, the S2 state can also be involved in this regard because, as is described in Gouterman's 4-orbital model,^[21] the Q- and B-band energies are

Table 4. The Δ HOMO (Δ H) and Δ LUMO (Δ L) values, the percentage contribution to the Q ($Q^{4ob\%}$) and B ($B^{4ob\%}$) bands of the one-electron transitions that link the lower-energy MO derived from the parent perimeter HOMO to the MOs derived from the LUMO, the calculated Q- and B-band intensities (Q^{int} , B^{int}), and wavelengths (Q^{calcd} , B^{calcd}) derived from ZINDO/s calculations.

	Δ H	Δ L	$Q^{4ob\%}$	$B^{4ob\%}$	Q^{int}	B^{int}	Q^{calcd}	B^{calcd}
$C_{18}H_{18}$	0.00	0.00	96, 97	97, 97	0.00, 0.00	4.51, 4.51	898, 677	359, 359
P	0.36	0.02	96, 97	77, 95	0.03, 0.05	1.75, 2.30	743, 657	383, 369
TPP	0.10	0.04	96, 97	88, 94	0.00, 0.00	2.56, 2.89	784, 691	405, 400
6i	0.07	0.02	92, 93	86, 91	0.00, 0.00	2.81, 3.07	796, 702	416, 413
TBP	1.19	0.26	96, 96	86, 92	0.19, 0.42	2.61, 2.28	807, 775	405, 378
TPTBP	0.72	0.33	95, 96	91, 93	0.05, 0.26	2.72, 2.52	880, 828	451, 428
TPTANP	0.09	0.06	88, 84	55, 44	0.01, 0.06	0.80, 1.07	685, 546	515, 496
5a	0.14	0.05	92, 94	83, 91	0.01, 0.01	1.40, 1.85	1016, 885	550, 537
5i	0.38	0.07	92, 94	86, 91	0.05, 0.05	1.56, 1.87	1040, 902	555, 552
$C_{16}H_{16}^{2<M->}$	0.00	0.00	96, 96	97, 97	0.00, 0.00	3.70, 3.70	724, 724	350, 350
ZnP	0.62	0.00	96, 96	94, 94	0.07, 0.06	2.31, 2.31	674, 674	367, 367
ZnTPP	0.11	0.00	96, 96	94, 94	0.00, 0.00	2.82, 2.82	704, 704	400, 400
ZnDPP	0.03	0.01	96, 96	91, 91	0.00, 0.00	2.86, 2.87	752, 752	428, 428
ZnTBP	1.44	0.00	94, 94	92, 92	0.35, 0.35	2.47, 2.47	770, 770	382, 382
ZnTPTBP	0.96	0.00	95, 95	93, 93	0.18, 0.18	2.55, 2.55	812, 812	430, 430
ZnTNP	1.82	0.00	95, 95	78, 78	0.57, 0.57	2.93, 2.93	850, 850	392, 392
ZnTPTNP	1.35	0.00	93, 93	67, 67	0.37, 0.37	1.53, 1.54	886, 886	449, 449
ZnTANP	0.52	0.00	89, 89	75, 75	0.16, 0.16	2.11, 2.11	762, 762	465, 465
ZnTPTANP	0.03	0.00	91, 91	90, 90	0.00, 0.00	2.33, 2.34	840, 840	514, 514
ZnTPhenP	0.78	0.01	93, 93	88, 87	0.20, 0.19	2.67, 2.67	772, 771	430, 430
Zn 5a	0.06	0.00	94, 93	90, 90	0.00, 0.00	1.78, 1.78	906, 906	534, 533

Table 5. The first oxidation (ox.) and first reduction (red.) potentials [V] of porphyrinoid compounds relative to the saturated calomel electrode and a comparison of trends in the ΔE_{o-r} [eV] values, the HOMO (H) and LUMO (L) energies [eV] in B3LYP geometry optimizations, the HOMO–LUMO bandgap ($|H-L|$), and the average observed and TD-DFT-calculated Q_{00} -band energies [eV].

	Solvent	1st ox.	1st red.	ΔE_{o-r}	Ref.	H	L	$ H-L $	$Q_{(calcd)}$	$Q_{(obs)}$
P	CH_2Cl_2	+0.94 ^[a]	−1.36 ^[a]	2.30 ^[a]	[50a]	−5.30	−2.24	3.06	2.37	2.19 ^[a]
TPP	CH_2Cl_2	+1.00	−1.23	2.23	[50b]	−4.91	−2.19	2.72	2.24	2.12
6i	CH_2Cl_2	+0.44	−1.38	1.82	[50c]	−4.22	−1.75	2.47	2.13	2.02
TBP	DMSO	+0.55	−1.13	1.68	[50d]	−4.69	−2.26	2.43	1.95	2.15
5a	CH_2Cl_2	+0.90	−0.93	1.83	^[b]	−4.47	−2.58	1.89	1.59	1.57
5i	CH_2Cl_2	+0.48	−0.89	1.37	^[b]	−3.74	−2.08	1.66	1.43	1.32
ZnP	CH_2Cl_2	+0.72 ^[a]	−1.33 ^[a]	2.05 ^[a]	[50a]	−5.21	−2.14	3.07	2.46	2.22
ZnTPP	CH_2Cl_2	+0.80	−1.35	2.15	[50b]	−4.98	−2.12	2.86	2.33	2.12
ZnDPP	CH_2Cl_2	+0.48	−1.34	1.82	[50e]	−4.72	−2.23	2.49	2.05	1.95
ZnTBP	DMSO	+0.38	−1.46	1.84	[50d]	−4.62	−2.10	2.52	2.05	1.98

[a] Redox data for P and ZnP are derived from free-base and zinc octaethylporphyrin, since comparatively little research has been carried out on the parent unsubstituted porphyrin. [b] This work.

Table 6. The first and second reduction (1st red., 2nd red.) and oxidation (1st ox., 2nd ox.) potentials [V] relative to the saturated calomel electrode, the gap between the first oxidation and reduction potentials (ΔE_{o-r}) and the Hammett parameters (σ_p)^[53] of TPTPhenP compounds in CH_2Cl_2 .

	$4\sigma_p$	2nd red. ^[a]	1st red. ^[a]	1st ox. ^[a]	2nd ox. ^[a]	ΔE_{o-r} ^[d]	$Q^{[e]}$	$B^{[e]}$
5i −N- (CH_3) ₂	−3.32	−	−0.89 ^[b]	0.48 ^[c]	0.92 ^[c]	1.37	1.34	2.02
5b −CH ₃	−0.68	−	−1.13 ^[b]	0.82 ^[c]	−	1.95	1.55	2.13
5a −H	0.00	−	−0.93 ^[b]	0.90 ^[c]	−	1.83	1.57	2.16
5f −I	0.72	−	−0.92 ^[b]	0.90 ^[c]	−	1.82	1.55	2.12
5e −Br	0.92	−	−0.96 ^[b]	0.84 ^[c]	1.16 ^[c]	1.80	1.55	2.14
5h −NO ₂	3.12	−1.50 ^[c]	−0.99 ^[b]	0.78 ^[c]	1.32 ^[c]	1.77	1.54	2.06

[a] Peak potentials were determined based on differential pulse voltammetry experiments. [b] Reversible peak. [c] Irreversible peak. [d] The gap between the first oxidation and reduction potentials (ΔE_{o-r}) [eV]. [e] The observed energies of the Q and B bands [eV].

determined by configurational interaction between four spin-allowed $\pi-\pi^*$ excited states, which arise from four one-electron transitions between the two MOs derived from the HOMO of the $C_{16}H_{16}^{2-}$ parent perimeter and the two MOs derived from the LUMO. When Δ HOMO \approx Δ LUMO \approx 0, however, as is predicted to be the case for TPTPhenPs (Figure 12), there are close to fully forbidden Q bands and fully allowed B bands based on the $\Delta M_L = \pm 1$ and ± 9 properties of the Q and B transitions. When there is only limited configurational interaction between the B and higher $\pi-\pi^*$ states, it is reasonable to expect that the B-band energy will be modified in a readily predictable manner when the *para* substituent of the phenyl groups on the *meso*-carbon atoms is changed based on a consideration of the nodal patterns of the four key frontier π MOs using a perimeter model approach. Kadish and Morrison^[52] demonstrated in the context of (*p*-X)TPP compounds that an increase in the electron-donating properties causes a negative shift in the reduction and oxidation potentials. Similar negative shifts are observed for (*p*-X)TPTPhenPs (Figure 14 and Table 6) and are consistent with a destabilization of both

the HOMO and LUMO. A consideration of the nodal properties makes it clear that the HOMO, LUMO, and LUMO+1 are more likely to be destabilized than the HOMO−1 (Figure 14), since there are large MO coefficients on the *meso*-carbon atoms. The negative shift is more marked in the case of the oxidation potential (Figure 13), since all four *meso*-carbon atoms lie on nodal planes or antinodes of the HOMO−1 and HOMO, respectively, due to the alignment of mirror planes along the *x* and *y* axes and the $\Delta M_L = \pm 4$ nodal properties of the MOs derived from the HOMO of the 16-atom parent hydrocarbon perimeter (Figures 10 and 14). In contrast, the *meso*-carbon atoms lie between the nodal planes of the LUMO and LUMO+1 due to the $\Delta M_L = \pm 5$ nodal properties, so the MO coefficients are smaller than is the case with the HOMO.

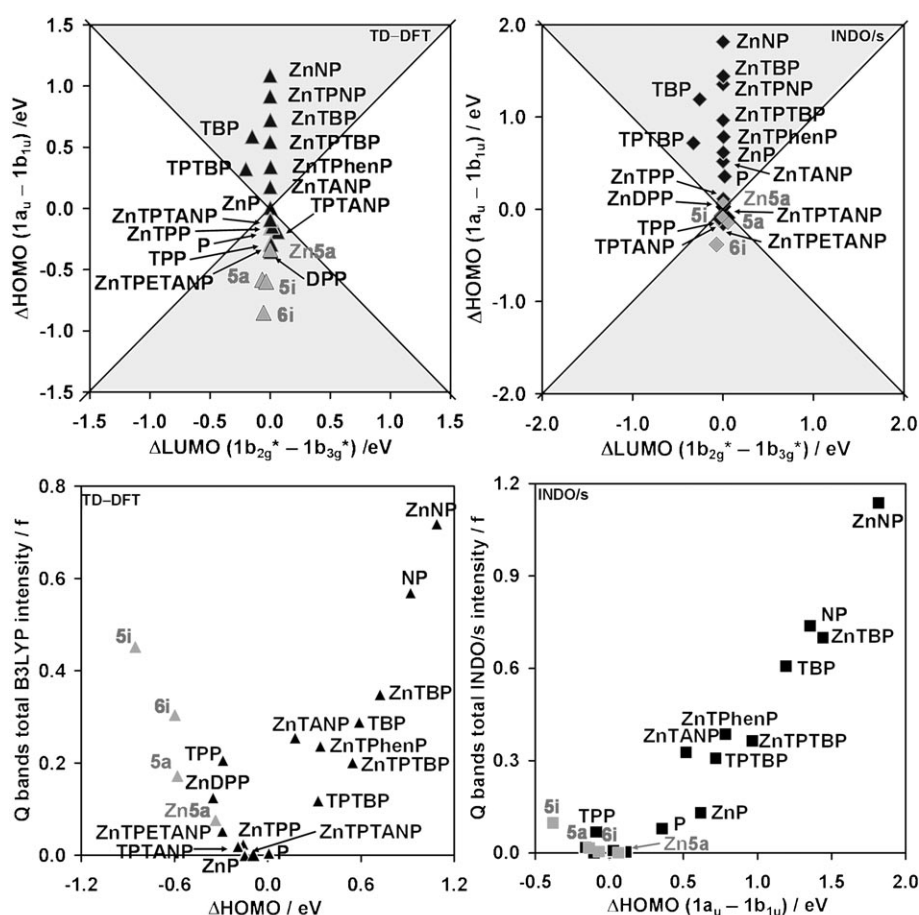


Figure 12. The effect of structural perturbations on the ΔHOMO and ΔLUMO values predicted by (top left) B3LYP and by (top right) INDO/s calculations for the same set of B3LYP-optimized geometries. In the light-gray shaded areas in which $\Delta\text{HOMO} > \Delta\text{LUMO}$, a $-ve/+ve$ MCD sign sequence is anticipated^[20] for the Q band in ascending energy terms, whereas a $+ve/-ve$ sign sequence is anticipated in the unshaded areas in which $\Delta\text{LUMO} > \Delta\text{HOMO}$. Bottom right: The calculated Q-band oscillator strengths from TD-DFT and (bottom left) INDO/s and calculations based on 6-31G(d) basis sets plotted against the ΔHOMO value. As the ΔHOMO value increases, the calculated oscillator strength increases. A greater destabilization of the $1b_{1u}$ MO (Figure 1) tends to be predicted in the TD-DFT calculations, thereby resulting in significantly greater calculated oscillator strengths for TPTPhenPs.

The B-band energies of **5b** and **5i** do not lie on the trend line formed by the energies of the electron-withdrawing substituents (Figure 13). This is not surprising, since Kadish and Morrison^[52] reported that the closest agreement with the $E_{1/2}$ versus $4\sigma_p$ trend was observed with electron-accepting substituents. Marked differences are observed in the spectra of these compounds relative to those of **5a** and **5c-f** (Figures 5 and 6). There is a marked intensification of the Q-band region of the **5b** and **5i** spectra, which may be related in part to increased vibrational band intensity caused by the $-\text{CH}_3$ and $-\text{N}(\text{CH}_3)_2$ groups. The presence of vibrational bands in the B-band region could significantly alter the position of the observed B-band centers in the absorption spectrum, which results from the overlap of the symmetry-split x - and y -polarized B_{00} bands. In the context of **5i**, there is a strong mesomeric interaction between the nitrogen lone pairs of $-\text{N}(\text{CH}_3)_2$ with the π system of the core porphyrinoid macrocycle (Figure 10) in addition to the inductive ef-

fects that are responsible for the trend observed with **5a** and **5c-f**. Michl has demonstrated that electron-donating substituents tend to have a greater effect on the ΔHOMO value due to the presence of additional high-lying occupied MOs with symmetry similar to those of the MOs derived from the HOMO of the parent hydrocarbon perimeter (Figure 10).^[20b] The mixing of these MOs due to the mesomeric effect, therefore, significantly modifies the energies of the frontier π MOs relative to **5a** and **5c-f** in which an inductive substituent effect is the dominant factor. The redox properties and the energies of the Q and B bands are, therefore, modified significantly.

In the context of the mesomeric interactions of the electron-accepting $-\text{CN}$ and $-\text{NO}_2$ substituents in **5g** and **5h**, there is less scope for a significant ΔLUMO value to be introduced because of the introduction of additional low-lying unoccupied MOs, due to the manner in which the alignment of the nodal planes of the four key frontier π MOs is determined by the planes of symmetry, which are introduced along the x and y axes by the saddling of the ligand and the protonation

of two pyrrole nitrogen atoms. In the context of the LUMO and LUMO+1, there are significant MO coefficients on the *meso*-carbon atoms, so there is less scope for the introduction of a significant ΔLUMO value based on the electron-withdrawing or -donating properties of the four aryl groups (Figure 14). The protonated and nonprotonated pyrrole nitrogen atoms are the positions on the inner ligand perimeter in which there is most scope for substantially modifying the ΔLUMO value based on the alignment of nodes and antinodes along the x and y axes in the LUMO and LUMO+1. Electron-accepting aryl substituents, such as $-\text{CN}$ and $-\text{NO}_2$, draw electron density away from these atoms, however, thereby minimizing the effect of the electronegativity difference on these atoms due to protonation.

The large ΔHOMO value that is introduced (Figure 12) in the electronic structure of **5i** causes increased mixing of the allowed and forbidden properties of the Q and B bands, so the Q bands gain significant intensity. Previous studies on a

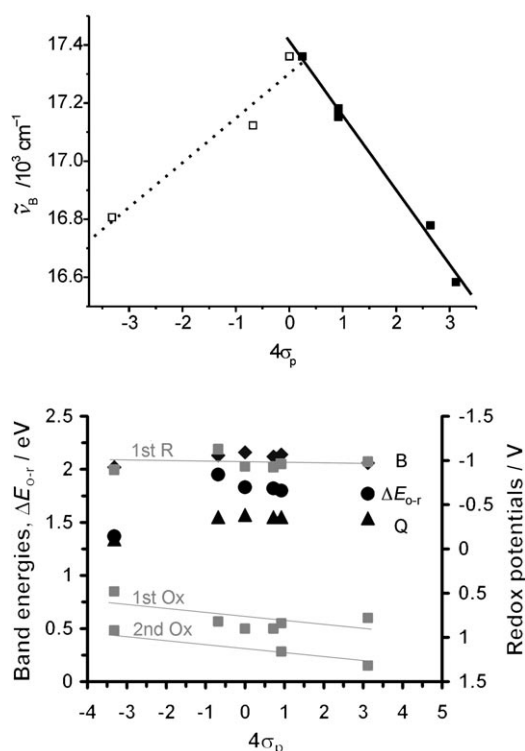


Figure 13. Plot of the B absorption-band energy in CHCl_3 versus Hammett parameter σ_p ($4\sigma_p$ because four substituents are attached to the porphyrin) for dyes **5c-h** with electron-withdrawing substituents (black squares) and **5a, 5b, and 5i** (top; white squares). The solid line represents a fit of the data ($r=0.996$) based on a linear regression analysis. The trends observed in the Q-band region broadly mirror those observed for the B band, but the correlation factor is considerably lower since there are substantially greater changes in the relative intensities and separations of the *x*- and *y*-polarized Q_{00} bands (Figures 5 and 6). Bottom: The observed Q- and B-band wavelengths and ΔE_{o-r} values [eV] denoted by black triangles, diamonds and circles, respectively, and plotted versus $4\sigma_p$. Redox potentials for the oxidation and reduction steps relative to the saturated calomel electrode are plotted as light gray squares against a secondary axis.

wide range of different radially symmetric fused-ring-expanded porphyrinoids have demonstrated that when $\Delta\text{HOMO} > \Delta\text{LUMO}$ there tends to be an increase in the level of configurational interaction between the B and

higher-energy $\pi-\pi^*$ states, thereby resulting in a blueshift of the B band and an increase in the energy gap between the Q and B bands.^[19] The increased energy separation of the Q and B bands, and the broadening and loss of intensity of the B band of **5i** (Figures 5 and 12) is consistent with this. From the standpoint of NIR dye applications, the properties of the Q bands of TPTPhenPs are considerably more important than those of the B band, however, since they lie at the red end of the visible region. The ability to fine-tune the band centers and intensities of the Q_{00} bands by varying the Hammett parameter of the *para* substituent and by introducing electron-donating substituents with a strong mesomeric interaction with the TPTPhenP chromophore should greatly facilitate the design of TPTPhenPs suitable for specific practical applications.

Conclusion

Substituted TPTPhenPs exhibit the most highly redshifted B and Q bands to have been reported to date for radially symmetric tetrapyrrole porphyrinoids. The optical properties of TPTPhenP compounds can be fine-tuned by carrying out the synthesis with different benzaldehydes so that *meso*-aryl groups with strongly electron-withdrawing or -donating properties are introduced into the π system. An unprecedented redshift of the Q band is observed for **5i** based on the strong electron-donating properties of the $-\text{N}(\text{CH}_3)_2$ groups, due to a marked destabilization of the HOMO and hence a decrease in the HOMO–LUMO bandgap. An increase in the ΔHOMO value (Table 4 and Figure 12) results in a further marked intensification of the Q_{00} bands and a significantly greater separation of the Q and B bands (Figures 11 and 12), since there is a greater level of configurational interaction between the B and higher-energy $\pi-\pi^*$ states. The protonated species of TPTPhenPs exhibit bathochromic shifts of the B and Q_{00} bands of up to 150 nm compared to the *meso*-unsubstituted TPhenPH₂²⁺ parent compound. The redshift of the lowest-energy of **5iH₃³⁺** (Figure 7) is an unprecedented 550 nm relative to the spectrum of TPP. These are by far the largest bathochromic shifts observed for a radially symmetric tetrapyrrole por-

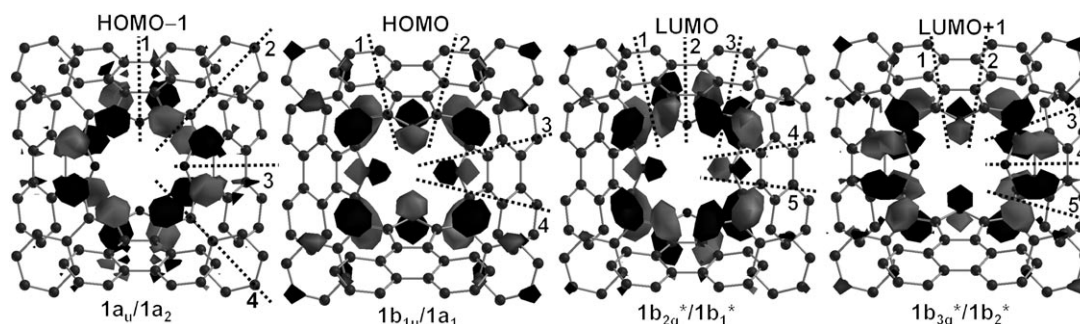


Figure 14. The alignment of the nodal planes in the four frontier π MOs of **5a** based on the $M_L = \pm 4$ and ± 5 properties of the parent $\text{C}_{16}\text{H}_{16}^{2-}$ parent perimeter. MO labels are shown for both D_{2h} and C_{2v} symmetry to aid comparison with higher-symmetry porphyrinoids (Figure 1). The protonated pyrrole nitrogen atoms are aligned with the vertical *y* axis in the plane of the page, whereas the *z* axis points out of the page towards the reader.

phyrinoid. Acid–base chemistry in conjunction with potent donor/acceptor groups can enable unprecedented NIR dye properties, which respond in a pre-designed way to a specific chemical input. These properties could lead to applications as precursors or building blocks for the construction of NIR-active supramolecular ensembles suitable for use in nonlinear optics, opto-electronics, solar-energy conversion, or as photosensitizers for photodynamic therapy. Still larger bathochromic shifts may still be achievable. The close correspondence observed in the trends predicted by TD-DFT and ZINDO/s calculations and those observed experimentally by optical spectroscopy and electrochemistry (Figure 11) demonstrate that this question can be approached based on rational design rather than by trial and error.

Experimental Section

General: Unless otherwise noted, all chemicals and solvents were of analytical reagent grade and used as received. Dry CH_2Cl_2 was freshly distilled over CaH_2 under nitrogen. Dry tetrahydrofuran (THF) was distilled from sodium/benzophenone under nitrogen. Column chromatography and TLC were performed using C-200 and Kieselgel 60 F254 instruments, respectively. ^1H and ^{13}C NMR spectra were acquired in $[\text{D}_7]\text{DMF}$ or CDCl_3 using a Bruker DRX500 spectrometer operating at 500 MHz for ^1H and 125 MHz for ^{13}C . Chemical shifts are reported in units of ppm and are referenced using TMS as the internal standard. MALDI-TOF mass spectra were recorded using a Bruker Autoflex IITM spectrometer. Elemental analyses for C, H, and N were performed using a Perkin–Elmer 240C elemental analyzer. Melting points were determined using a Reichert thermometer without correction. IR spectra were recorded using a VECTOR 22 spectrophotometer with KBr discs in the 4000–400 cm^{-1} region. The redox data were obtained using a Zahner Electrochemical Workstation. Data were measured for **5a**, **5b**, **5c**, **5f**, **5h**, and **5i** using a platinum working electrode, a platinum wire counter electrode, and an Ag/AgCl reference electrode using Fc/Fc^+ as an internal standard. The measurements were carried out in CH_2Cl_2 solution using 0.1 M Bu_4NPF_6 supporting electrolyte. All experiments were carried out under an argon atmosphere.

Synthesis: Phenanthro[9,10-*c*]pyrrole,^[30] ethyl isocyanoacetate,^[54] and 4-iodobenzaldehyde^[55] were prepared according to literature methods.

Porphyrin 5a: Benzaldehyde (106 mg, 1 mmol) was added to a stirred solution of phenanthro[9,10-*c*]pyrrole (217 mg, 1 mmol) in dry CH_2Cl_2 (350 mL), and the resulting solution was purged with argon for 10 min. The solution was cooled to -50°C and kept in the dark. $\text{BF}_3\cdot\text{Et}_2\text{O}$ (40 μL , 0.32 mmol) was added. The solution was stirred at -50°C for 2 h, warmed to room temperature, and stirred for another 48 h. Three drops of triethylamine were added followed by the addition of DDQ (227 mg, 1 mmol). After stirring for an additional 1 h, the solvents were removed under reduced pressure. The residue was purified by column chromatography on silica gel, eluting gradually from 50% chloroform/petroleum ether to CHCl_3 . The product was collected as a deep-red fraction. Recrystallization from CHCl_3 /methanol afforded **5a** as dark red solids in 17% yield (52 mg). M.p. $>300^\circ\text{C}$; ^1H NMR (500 MHz, $[\text{D}_7]\text{DMF}$): $\delta = 1.11$ (b, 2H), 6.93 (m, 8H), 7.36–7.38 (m, 8H), 7.71–7.74 (m, 12H), 7.95–7.97 (m, 8H), 8.59–8.63 (m, 8H), 8.98 ppm (m, 8H); IR (KBr): $\tilde{\nu}_{\text{max}} = 3424, 3081, 1629, 1443, 1352, 1048, 759, 726 \text{ cm}^{-1}$; MS (MALDI-TOF): m/z : 1216.6 $[\text{M}+\text{H}^+]$; elemental analysis calcd (%) for $\text{C}_{92}\text{H}_{54}\text{N}_4$: C 90.91, H 4.48, N 4.61; found: C 90.80, H 4.60, N 4.42.

Porphyrin 5b: Compound **5b** was prepared as described above from *p*-tolyl aldehyde (120 mg, 1 mmol), phenanthro[9,10-*c*]pyrrole (217 mg, 1 mmol), $\text{BF}_3\cdot\text{Et}_2\text{O}$ (40 μL , 0.32 mmol), and DDQ (227 mg, 1 mmol) in dry CH_2Cl_2 (350 mL). Chromatography on silica, eluting gradually from 50% CHCl_3 /petroleum ether to CHCl_3 , followed by recrystallization

from CHCl_3 /methanol, afforded **5b** as dark red crystals in 11% yield (35 mg). M.p. $>300^\circ\text{C}$; ^1H NMR (500 MHz, $[\text{D}_7]\text{DMF}$): $\delta = 1.01$ (b, 2H), 2.44 (s, 12H), 6.83 (m, 8H), 7.26 (m, 8H), 7.48–7.50 (m, 8H), 8.27 (m, 8H), 8.47 (m, 8H), 8.73 ppm (m, 8H); IR (KBr): $\tilde{\nu}_{\text{max}} = 3425, 3086, 1604, 1445, 1352, 1079, 1047, 758, 728 \text{ cm}^{-1}$; MS (MALDI-TOF): m/z : 1271.41 $[\text{M}^+]$; elemental analysis calcd (%) for $\text{C}_{96}\text{H}_{62}\text{N}_4$: C 90.68, H 4.91, N 4.41; found: C 90.65, H 4.89, N 4.86.

Porphyrin 5c: Compound **5c** was prepared as described above from *p*-fluorobenzaldehyde (124 mg, 1 mmol), phenanthro[9,10-*c*]pyrrole (217 mg, 1 mmol), $\text{BF}_3\cdot\text{Et}_2\text{O}$ (40 μL , 0.32 mmol), and DDQ (227 mg, 1 mmol) in CH_2Cl_2 (350 mL). Column chromatography on silica gel, eluting gradually from 40% CHCl_3 /petroleum ether to chloroform, followed by recrystallization from CHCl_3 /methanol, afforded **5c** as a dark red powder in 10% yield (32 mg). M.p. $>300^\circ\text{C}$; ^1H NMR (500 MHz, $[\text{D}_7]\text{DMF}$): $\delta = 0.89$ (b, 2H), 6.91–6.94 (m, 8H), 7.46–7.49 (m, 8H), 7.60–7.63 (m, 8H), 7.86–7.88 (m, 8H), 8.65–8.67 (m, 8H), 8.86–8.88 ppm (m, 8H); IR (KBr): $\tilde{\nu}_{\text{max}} = 3426, 3086, 1597, 1449, 1352, 1158, 1048, 758, 724 \text{ cm}^{-1}$; MS (MALDI-TOF): m/z : 1288.4 $[\text{M}^+]$; elemental analysis calcd (%) for $\text{C}_{92}\text{H}_{50}\text{F}_4\text{N}_4$: C 85.83, H 3.91, N 4.35; found: C 85.86, H 3.88, N 4.21.

Porphyrin 5d: Compound **5d** was prepared as described above from *p*-chlorobenzaldehyde (140 mg, 1 mmol), phenanthro[9,10-*c*]pyrrole (217 mg, 1 mmol), $\text{BF}_3\cdot\text{Et}_2\text{O}$ (40 μL , 0.32 mmol), and DDQ (227 mg, 1 mmol) in CH_2Cl_2 (350 mL). Column chromatography on silica gel, eluting gradually from 40% CHCl_3 /petroleum ether to 1% triethylamine/chloroform, followed by recrystallization from CHCl_3 /methanol, afforded **5d** as a dark red powder in 13% yield (44 mg). M.p. $>300^\circ\text{C}$; ^1H NMR (500 MHz, $[\text{D}_7]\text{DMF}$): $\delta = 0.84$ (b, 2H), 7.02–7.05 (m, 8H), 7.42–7.44 (m, 8H), 7.57–7.59 (m, 8H), 7.78–7.81 (m, 8H), 8.68–8.71 (m, 8H), 8.92–8.95 ppm (m, 8H); IR (KBr): $\tilde{\nu}_{\text{max}} = 3421, 3084, 1586, 1447, 1350, 1047, 1092, 758, 726 \text{ cm}^{-1}$; MS (MALDI-TOF): m/z : 1353.3 $[\text{M}+\text{H}^+]$; elemental analysis calcd (%) for $\text{C}_{92}\text{H}_{50}\text{Cl}_4\text{N}_4$: C 81.66, H 3.72, N 4.14; found: C 81.45, H 3.80, N 4.21.

Porphyrin 5e: Compound **5e** was prepared as described above from 4-bromobenzaldehyde (185 mg, 1 mmol), phenanthro[9,10-*c*]pyrrole (217 mg, 1 mmol), $\text{BF}_3\cdot\text{Et}_2\text{O}$ (40 μL , 0.32 mmol), and DDQ (227 mg, 1 mmol). Column chromatography on silica gel, eluting gradually from 50% CHCl_3 /petroleum ether to CHCl_3 , followed by recrystallization from CHCl_3 /methanol, afforded **5e** as a dark red powder in 11% yield (42 mg). M.p. $>300^\circ\text{C}$; ^1H NMR (500 MHz, $[\text{D}_7]\text{DMF}$): $\delta = 0.86$ (b, 2H), 6.99–7.03 (m, 8H), 7.40–7.43 (m, 8H), 7.55–7.59 (m, 8H), 7.83–7.86 (m, 8H), 8.66–8.69 (m, 8H), 8.85–8.88 ppm (m, 8H); IR (KBr): $\tilde{\nu}_{\text{max}} = 3422, 3082, 1630, 1442, 1350, 1077, 1047, 759, 725 \text{ cm}^{-1}$; MS (MALDI-TOF): m/z : 1531.1 $[\text{M}^+]$; elemental analysis calcd (%) for $\text{C}_{92}\text{H}_{50}\text{Br}_4\text{N}_4$: C 72.17, H 3.29, N 3.66; found: C 72.17, H 3.36, N 3.57.

Porphyrin 5f: Compound **5f** was prepared as described above from 4-iodobenzaldehyde (232 mg, 1 mmol), phenanthro[9,10-*c*]pyrrole (217 mg, 1 mmol), $\text{BF}_3\cdot\text{Et}_2\text{O}$ (40 μL , 0.32 mmol), and DDQ (227 mg, 1 mmol). Column chromatography on silica gel, eluting gradually from 40% CHCl_3 /petroleum ether to 80% CHCl_3 /petroleum ether, followed by recrystallization from CHCl_3 /methanol, afforded **5f** as a dark red powder in 15% yield (65 mg). M.p. $>300^\circ\text{C}$; ^1H NMR (500 MHz, $[\text{D}_7]\text{DMF}$): $\delta = 0.82$ (b, 2H), 6.98–7.05 (m, 8H), 7.19–7.25 (m, 8H), 7.38–7.46 (m, 8H), 7.57–7.63 (m, 8H), 8.02–8.10 (m, 8H), 8.67–8.72 ppm (m, 8H); IR (KBr): $\tilde{\nu}_{\text{max}} = 3424, 3080, 1576, 1446, 1348, 1060, 758, 727, 617 \text{ cm}^{-1}$; MS (MALDI-TOF): m/z : 1718.9 $[\text{M}^+]$; elemental analysis calcd (%) for $\text{C}_{92}\text{H}_{50}\text{I}_4\text{N}_4$: C 64.28, H 2.93, N 3.26; found: C 64.13, H 3.01, N 3.15.

Porphyrin 5g: Compound **5g** was prepared as described above from 4-cyanobenzaldehyde (131 mg, 1 mmol), phenanthro[9,10-*c*]pyrrole (217 mg, 1 mmol), $\text{BF}_3\cdot\text{Et}_2\text{O}$ (40 μL , 0.32 mmol), and DDQ (227 mg, 1 mmol). Chromatography on silica, eluting gradually from 50% CHCl_3 /petroleum ether to CHCl_3 , followed by recrystallization from CHCl_3 /methanol, afforded **5g** as dark red crystals in 14% yield (49 mg). M.p. $>300^\circ\text{C}$; ^1H NMR (500 MHz, $[\text{D}]\text{TFA}/\text{CDCl}_3$): $\delta = 0.89$ (b, 2H), 6.86 (t, $J_1 = 7.5 \text{ Hz}$, $J_2 = 8.0 \text{ Hz}$, 8H), 7.19 (d, $J = 8.0 \text{ Hz}$, 8H), 7.42 (t, $J_1 = 7.5 \text{ Hz}$, $J_2 = 8.0 \text{ Hz}$, 8H), 7.94 (d, $J = 7.5 \text{ Hz}$, 8H), 8.48 (d, $J = 8.5 \text{ Hz}$, 8H), 8.89 ppm (d, $J = 8.5 \text{ Hz}$, 8H); IR (KBr): $\tilde{\nu}_{\text{max}} = 3386, 3084, 2225, 1599, 1446, 1343, 1166, 759, 725 \text{ cm}^{-1}$; MS (MALDI-TOF): m/z : 1315.4 $[\text{M}^+]$; elemental

analysis calcd (%) for $C_{96}H_{50}N_8$: C 87.65, H 3.83, N 8.52; found: C 87.51, H 3.87, N 8.44.

Porphyrin 5h: Compound **5h** was prepared as described above from 4-nitrobenzaldehyde (151 mg, 1 mmol), phenanthro[9,10-c]pyrrole (217 mg, 1 mmol), $BF_3 \cdot Et_2O$ (40 μ L, 0.32 mmol), and DDQ (227 mg, 1 mmol). Chromatography on silica gel, eluting gradually from 50% $CHCl_3$ /petroleum ether to $CHCl_3$, followed by recrystallization from $CHCl_3$ /methanol, afforded **5h** as dark green crystals in 6% yield (21 mg). M.p. > 300 °C; 1H NMR (500 MHz, $[D_7]DMF$): δ = 0.83 (b, 2H), 7.01 (m, 8H), 7.39 (m, 8H), 7.51 (m, 8H), 8.53 (m, 8H), 8.69 (m, 8H), 9.21–9.28 ppm (m, 8H); IR (KBr): $\tilde{\nu}_{max}$ = 3417, 3084, 1588, 1515, 1354, 1337, 1046, 852, 758, 727 cm^{-1} ; MS (MALDI-TOF): m/z : 1396.4 $[M+H^+]$; elemental analysis calcd (%) for $C_{92}H_{50}N_8O_8$: C 79.19, H 3.61, N 8.03; found: C 79.13, H 3.49, N 8.03.

Porphyrin 5i: Compound **5i** was prepared as described above from 4-dimethylamino-benzaldehyde (149 mg, 1 mmol), phenanthro[9,10-c]pyrrole (217 mg, 1 mmol), $BF_3 \cdot Et_2O$ (45 μ L, 0.37 mmol), and DDQ (31 mg, 0.14 mmol). Chromatography on silica gel, eluting gradually from $CHCl_3$ to ethyl acetate, followed by recrystallization from $CHCl_3$ /methanol afforded **5i** as deep blue crystals in 19% yield (68 mg). M.p. > 300 °C; 1H NMR (500 MHz, $[D_7]DMF$): δ = 1.86 (b, 2H), 3.79 (s, 24H), 7.18 (m, 16H), 7.55 (d, 8H), 7.92 (d, 8H), 8.69 ppm (m, 16H); MS (MALDI-TOF): m/z : 1387.6 $[M^+]$; elemental analysis calcd (%) for $C_{100}H_{74}N_8$: C 86.55, H 5.37, N 8.07; found: C 86.42, H 5.31, N 8.05.

Optical spectroscopy: $CHCl_3$ and trifluoroacetic acid employed for the fluorescence measurements were of UV spectroscopic grade. $CHCl_3$ stabilized by 0.5% ethanol supplied by Nacalai Tesque was used for MCD measurements. Steady-state absorption and fluorescence measurements were carried out using a Cary 5000 UV/Vis-NIR spectrophotometer and a Spectronics Instrument 8100 spectrofluorometer. For all measurements, the temperature was kept constant at (298 ± 1) K. All absorption measurements were carried out in 50 mm cuvettes. Molar absorption coefficients were determined from $N=4$ independent solutions and only very dilute stock solutions (1–10 μ M) were used in these studies to avoid aggregation or solubility problems. The uncertainties of measurement amount to around $\pm 10\%$ for **5b** and **5d** and to $\pm 5\%$ for the other dyes. Fluorescence studies were performed in 10 mm cuvettes (90° standard geometry, polarizers set at 54.7° for emission and 0° for excitation) with optically dilute solutions with an absorbance between 0.05 and 0.1 at the maximum of the B band. The fluorescence quantum yields (Φ_f) were determined relative to cresyl violet in methanol ($\Phi_f = 0.61 \pm 0.01$).^[56] The fluorescence spectra presented here were spectrally corrected.^[57] The uncertainty of the Φ_f measurements were determined to be $\pm 20\%$. Fluorescence lifetimes (τ_f) were determined using a unique customized laser-pulse fluorometer with picosecond time resolution.^[56] The fluorescence was collected at right angles (polarizer set at 54.7°; monochromator with spectral bandwidths of 16 nm). While realizing typical instrumental response functions of full-width half-maximum (fwhm) of around (25–30) ps, the time division was 4.8 ps channel⁻¹ and the experimental accuracy amounted to ± 3 ps, respectively. The laser beam was attenuated using a double prism attenuator from LTB, and typical excitation energies were in the nanowatt to microwatt range (average laser power). The fluorescence lifetime profiles were analyzed using a PC with the Global Unlimited V2.2 software package (Laboratory for Fluorescence Dynamics, University of Illinois). The goodness-of-fit of the single decays as judged by reduced chi-squared (χ_R^2) and the autocorrelation function $C(j)$ of the residuals was always below $\chi_R^2 < 1.2$. The parallel spectrophotometric and MCD titrations were performed in $CHCl_3$ using a Hitachi U-3410 spectrophotometer and a Jasco J-725 spectrodichromometer coupled to a Jasco electromagnet that produces a magnetic field of up to 1.09 T using a 10 mm cuvette.

Calculations: Molecular structures were optimized for free-base and/or Zn^{II} complexes porphyrin (P), tetraphenylporphyrin (TPP), tetrabenzoporphyrin (TBP), tetraphenyltetrabenzoporphyrin (TPTBP), tetranaphthoporphyrin (TNP), tetraphenyltetranaphthoporphyrin (TPTNP), tetraacenaphthoporphyrin (TANP), tetraphenyltetraacenaphthoporphyrin (TPTANP), tetraphenanthroporphyrin (TPhenP), tetraphenyltetraphenanthroporphyrin (TPTPhenP, **5a**), and dodecaphenylporphyrin (DPP)

(Scheme 1), **5i**, $5iH_2^{2+}$, and the free-base (**6i**) and protonated species ($6iH_2^{2+}$, $6iH_3^{3+}$, $6iH_4^{4+}$, $6iH_4^{4+}_{adj}$, $6iH_4^{4+}_{opp}$, $6iH_5^{5+}$, $6iH_6^{6+}$) of a TPP model complex for **5i** (Scheme 2) through the use of the B3LYP functional of the Gaussian 03W software package^[32] by using 6-31G or 6-31G(d) basis sets. ZINDO/s and TD-DFT calculations were carried out based on B3LYP-optimized geometries.

Acknowledgements

Financial support from the National Natural Science Foundation of China (nos. 20971066 and 21021062), the Chinese Ministry of Education's Program for New Century Excellent Talents in Universities (no. NCET-08-0272), the Major State Basic Research Development Program of China (grant nos. 2011CB808704 and 2007CB925103), a Grant-in-Aid for Scientific Research on Innovative Areas (no. 20108007, "pi-Space") provided by the Japanese Ministry of Education, Culture, Sports, Science, and Technology (MEXT), the Alexander von Humboldt Foundation and the European Commission's Human Resources & Mobility Programme for a Marie Curie Intra-European Fellowship is highly appreciated. We thank D. Pfeifer (BAM Div. I.3) for help with protonation experiments by NMR spectroscopy, which were fruitless because of solubility problems.

- [1] a) R. Bonnett, *Chem. Soc. Rev.* **1995**, *24*, 19–33; b) Z. Zhang, G. M. Ferrence, T. D. Lash, *Org. Lett.* **2009**, *11*, 1249–1252; c) T. Lu, P. Shao, I. Mathew, A. Sand, W. Sun, *J. Am. Chem. Soc.* **2008**, *130*, 15782–15783; d) C. Comuzzi, S. Cogo, M. Overhand, G. A. Van der Marel, H. S. Overkleeft, L. E. Xodo, *J. Med. Chem.* **2006**, *49*, 196–204; e) M. Drobizhev, Y. Stepanenko, Y. Dzenis, A. Karotki, A. Rebane, P. N. Taylor, H. L. Anderson, *J. Phys. Chem. B* **2005**, *109*, 7223–7236.
- [2] a) C. Ikeda, N. Sakamoto, T. Nabeshima, *Org. Lett.* **2008**, *10*, 4601–4604; b) D. Wu, A. B. Descalzo, F. Weik, F. Emmerling, Z. Shen, X.-Z. You, K. Rurack, *Angew. Chem.* **2008**, *120*, 199–203; *Angew. Chem. Int. Ed.* **2008**, *47*, 193–197; c) X.-J. Zhu, S.-T. Fu, W.-K. Wong, J.-P. Guo, W.-Y. Wong, *Angew. Chem.* **2006**, *118*, 3222–3226; *Angew. Chem. Int. Ed.* **2006**, *45*, 3150–3154.
- [3] a) J. M. Lim, Z. S. Yoon, J.-Y. Shin, K. S. Kim, M.-C. Yoon, D. Kim, *Chem. Commun.* **2009**, 261–273; b) K. S. Kim, Z. S. Yoon, A. B. Ricks, J.-Y. Shin, S. Mori, J. Sankar, S. Saito, Y. M. Jung, M. R. Wasielewski, A. Osuka, D. Kim, *J. Phys. Chem. A* **2009**, *113*, 4498–4506; c) Z. S. Yoon, D.-G. Cho, K. S. Kim, J. L. Sessler, D. Kim, *J. Am. Chem. Soc.* **2008**, *130*, 6930–6931.
- [4] M. Calvete, G. Y. Yang, M. Hanack, *Synth. Met.* **2004**, *141*, 231–243.
- [5] a) D. Holten, D. F. Bocian, J. S. Lindsey, *Acc. Chem. Res.* **2002**, *35*, 57–69; b) X. He, H. Liu, Y. Li, Y. Liu, F. Lu, Y. Li, D. Zhu, *Macromol. Chem. Phys.* **2005**, *206*, 2199–2205; c) R. Iqbal, S. C. Moratti, A. B. Holmes, G. Yahioglu, L. R. Milgrom, F. Cacialli, J. Morgado, R. H. Friend, *J. Mater. Sci.: Mater. Electron.* **2000**, *11*, 97–103; d) R. W. Wagner, J. S. Lindsey, J. Seth, V. Palaniappan, D. F. Bocian, *J. Am. Chem. Soc.* **1996**, *118*, 3996–3997.
- [6] a) D. Wu, Z. Shen, Z.-L. Xue, X.-Z. You, *Chin. J. Inorg. Chem.* **2007**, *23*, 1–14; b) J. A. A. W. Elemans, R. Van Hameren, R. J. M. Nolte, A. E. Rowan, *Adv. Mater.* **2006**, *18*, 1251–1266; c) C.-P. Hsieh, H.-P. Lu, C.-L. Chiu, C.-W. Lee, S.-H. Chuang, C.-L. Mai, W.-N. Yen, S.-J. Hsu, E. W.-G. Diau, C.-Y. Yeh, *J. Mater. Chem.* **2010**, *20*, 1127–1134; d) S. Hayashi, M. Tanaka, H. Hayashi, S. Eu, T. Umeyama, Y. Matano, Y. Araki, H. Imahori, *J. Phys. Chem. C* **2008**, *112*, 15576–15585.
- [7] a) I. A. Maretina, *Russ. J. Gen. Chem.* **2009**, *79*, 1544–1581; b) H. L. Anderson, *Chem. Commun.* **1999**, 2323–2330. H. Zou, M. J. Therien, J. K. Blasie, *J. Phys. Chem. B* **2008**, *112*, 1350–1357; c) M. U. Winters, J. Karnbratt, M. Eng, C. J. Wilson, H. L. Anderson, B. Albinsson, *J. Phys. Chem. C* **2007**, *111*, 7192–7199; d) Z. Shen, H. Uno, Y. Shimizu, N. Ono, *Org. Biomol. Chem.* **2004**, *2*, 3442–3447; e) S. M. Kuebler, R. G. Denning, H. L. Anderson, *J. Am. Chem. Soc.*

- 2000, 122, 339–347; f) P. N. Taylor, A. P. Wylie, J. Huuskonen, H. L. Anderson, *Angew. Chem.* **1998**, 110, 1033–1037; *Angew. Chem. Int. Ed.* **1998**, 37, 986–989.
- [8] a) R. Misra, T. K. Chandrashekar, *Acc. Chem. Res.* **2008**, 41, 265–279; b) J. L. Sessler, D. Seidel, *Angew. Chem.* **2003**, 115, 5292–5333; *Angew. Chem. Int. Ed.* **2003**, 42, 5134–5175; c) J. S. Reddy, V. G. Anand, *J. Am. Chem. Soc.* **2009**, 131, 15433–15439; d) Y. Kamimura, S. Shimizu, A. Osuka, *Chem. Eur. J.* **2007**, 13, 1620–1628; e) Y. Inokuma, T. Matsunari, N. Ono, H. Uno, A. Osuka, *Angew. Chem.* **2005**, 117, 1890–1894; *Angew. Chem. Int. Ed.* **2005**, 44, 1856–1860.
- [9] a) S. Tokuji, T. Yurino, N. Aratani, H. Shinokubo, A. Osuka, *Chem. Eur. J.* **2009**, 15, 12208–12211; b) M. Siczek, P. J. Chmielewski, *Angew. Chem.* **2007**, 119, 7576–7580; *Angew. Chem. Int. Ed.* **2007**, 46, 7432–7436; c) H. Uno, Y. Kitawaki, N. Ono, *Chem. Commun.* **2002**, 116–117; d) T. Ogawa, Y. Nishimoto, N. Yoshida, N. Ono, A. Osuka, *Angew. Chem.* **1999**, 111, 140–142; *Angew. Chem. Int. Ed.* **1999**, 38, 176–179.
- [10] a) T. D. Lash, *J. Porphyrins Phthalocyanines* **2001**, 5, 267–288; b) T. D. Lash in *The Porphyrin Handbook, Vol. 2* (Eds.: K. M. Kadish, K. M. Smith, R. Guilard), Academic, New York, **1999**, Chapter 10, pp. 125–199, and references therein.
- [11] a) N. K. S. Davis, M. Pawlicki, H. L. Anderson, *Org. Lett.* **2008**, 10, 3945–3947; b) J. M. Manley, T. J. Roper, T. D. Lash, *J. Org. Chem.* **2005**, 70, 874–891; c) N. Ono, T. Yamamoto, N. Shimada, K. Kuroki, M. Wada, R. Utsunomiya, T. Yano, H. Uno, T. Murashima, *Heterocycles* **2003**, 61, 433–447.
- [12] R. E. Haddad, S. Gazeau, J. Pecaut, J. Marchon, C. J. Medforth, J. A. Shelnutt, *J. Am. Chem. Soc.* **2003**, 125, 1253–1268.
- [13] J. A. Shelnutt, X.-Z. Song, J.-G. Ma, S.-L. Jia, W. Jentzen, C. J. Medforth, *Chem. Soc. Rev.* **1998**, 27, 31–41.
- [14] S. A. Vinogradov, D. F. Wilson, *J. Chem. Soc. Perkin Trans. 2* **1995**, 103–111.
- [15] V. N. Kopranchikov, A. M. Vorotnikov, S. N. Dashkevich, E. A. Luk'yanets, *Russ. J. Gen. Chem.* **1985**, 55, 803–809.
- [16] J. D. Spence, T. D. Lash, *J. Org. Chem.* **2000**, 65, 1530–1539.
- [17] N. Ono, H. Hironaga, K. Ono, S. Kaneko, T. Murashima, T. Ueda, C. Tsukamura, T. Ogawa, *J. Chem. Soc. Perkin Trans. 1* **1996**, 417–423.
- [18] T. D. Lash, P. Chandrasekar, *J. Am. Chem. Soc.* **1996**, 118, 8767–8768.
- [19] J. Mack, Y. Asano, N. Kobayashi, M. J. Stillman, *J. Am. Chem. Soc.* **2005**, 127, 17697–17711.
- [20] a) J. Michl, *J. Am. Chem. Soc.* **1978**, 100, 6801–6811; b) J. Michl, *Tetrahedron* **1984**, 40, 3845–3934.
- [21] M. Gouterman in *The Porphyrins, Vol. 3* (Ed.: D. Dolphin), Academic, New York, **1978**, pp. 1–165.
- [22] H.-J. Xu, Z. Shen, T. Okujima, N. Ono, X.-Z. You, *Tetrahedron Lett.* **2006**, 47, 931–934.
- [23] J. Mack, M. J. Stillman, N. Kobayashi, *Coord. Chem. Rev.* **2007**, 251, 429–453.
- [24] a) W. J. Moffitt, *J. Chem. Phys.* **1954**, 22, 320–333; b) W. J. Moffitt, *J. Chem. Phys.* **1954**, 22, 1820–1829.
- [25] a) J. Mack, M. J. Stillman in *The Porphyrin Handbook, Vol. 16* (Eds.: K. Kadish, K. Smith, R. Guilard), Academic, New York, **2003**, Chapter 103, pp. 43–116; b) J. Mack, M. J. Stillman, *Coord. Chem. Rev.* **2001**, 219–221, 993–1032.
- [26] M. H. Perrin, *J. Chem. Phys.* **1973**, 59, 2090–2104.
- [27] J. Mack, M. Bunya, Y. Shimizu, H. Uoyama, N. Komobuchi, T. Okujima, H. Uno, S. Ito, M. J. Stillman, N. Ono, N. Kobayashi, *Chem. Eur. J.* **2008**, 14, 5001–5020.
- [28] T. Fukuda, S. Homma, N. Kobayashi, *Chem. Eur. J.* **2005**, 11, 5205–5216.
- [29] a) J. S. Lindsey, I. C. Schreiman, H. C. Hsu, P. C. Kearney, A. M. Marguerettaz, *J. Org. Chem.* **1987**, 52, 827–836; b) J. S. Lindsey, R. W. Wagner, *J. Org. Chem.* **1989**, 54, 828–836.
- [30] B. H. Novak, T. D. Lash, *J. Org. Chem.* **1998**, 63, 3998–4010.
- [31] T. D. Lash, B. H. Novak, *Angew. Chem.* **1995**, 107, 723–725; *Angew. Chem. Int. Ed. Engl.* **1995**, 34, 683–685.
- [32] Gaussian 03, Revision C02, M. J. Frisch, G. W. Trucks, H. B. Schlegel, G. E. Scuseria, M. A. Robb, J. R. Cheeseman, J. A. Montgomery, Jr., T. Vreven, K. N. Kudin, J. C. Burant, J. M. Millam, S. S. Iyengar, J. Tomasi, V. Barone, B. Mennucci, M. Cossi, G. Scalmani, N. Rega, G. A. Petersson, H. Nakatsuji, M. Hada, M. Ehara, K. Toyota, R. Fukuda, J. Hasegawa, M. Ishida, T. Nakajima, Y. Honda, O. Kitao, H. Nakai, M. Klene, X. Li, J. E. Knox, H. P. Hratchian, J. B. Cross, V. Bakken, C. Adamo, J. Jaramillo, R. Gomperts, R. E. Stratmann, O. Yazyev, A. J. Austin, R. Cammi, C. Pomelli, J. W. Ochterski, P. Y. Ayala, K. Morokuma, G. A. Voth, P. Salvador, J. J. Dannenberg, V. G. Zakrzewski, S. Dapprich, A. D. Daniels, M. C. Strain, O. Farkas, D. K. Malick, A. D. Rabuck, K. Raghavachari, J. B. Foresman, J. V. Ortiz, Q. Cui, A. G. Baboul, S. Clifford, J. Cioslowski, B. B. Stefanov, G. Liu, A. Liashenko, P. Piskorz, I. Komaromi, R. L. Martin, D. J. Fox, T. Keith, M. A. Al-Laham, C. Y. Peng, A. Nanayakkara, M. Challacombe, P. M. W. Gill, B. Johnson, W. Chen, M. W. Wong, C. Gonzalez, J. A. Pople, Gaussian, Inc., Wallingford CT, **2004**.
- [33] When shoulders appear on the low-energy side of the Q bands like in **5g** and **5h** (more prominently) and in **5d-f** (less prominently), the maxima of the respective 0,0 bands after spectral deconvolution on the energy scale have been used to calculate the Stokes shifts.
- [34] A. Harriman, R. J. Hsieh, *J. Chem. Soc. Faraday Trans. 2* **1981**, 77, 1695–1702.
- [35] S. Gentemann, C. J. Medforth, T. P. Forsyth, D. J. Nurco, K. M. Smith, J. Fajer, D. Holten, *J. Am. Chem. Soc.* **1994**, 116, 7363–7368.
- [36] N. S. Savenkova, R. T. Kuznetsova, I. N. Lapin, V. A. Svetlichnyi, G. V. Mayer, P. A. Shatunov, *Opt. Spectrosc.* **2005**, 99, 751–758.
- [37] W. Siebrand, *J. Chem. Phys.* **1967**, 46, 440–447.
- [38] $k_{nr} = (1 - \Phi_f) \times \tau_f^{-1}$.
- [39] R. Bonnett, A. Harriman, A. N. Kozyrev, *J. Chem. Soc. Faraday Trans.* **1992**, 88, 763–769.
- [40] a) A. T. Gradyushko, D. T. Kozhich, K. N. Solov'ev, M. P. Tsvirko, *J. Appl. Spectrosc.* **1970**, 12, 838–840; b) K. N. Solov'ev, M. P. Tsvirko, A. T. Gradyushko, D. T. Kozhich, *Opt. Spectrosc.* **1972**, 33, 480–483.
- [41] E. A. Borisevich, G. D. Egorova, V. N. Knyuksho, K. N. Solov'ev, *Opt. Spectrosc.* **1987**, 63, 34–37.
- [42] The formalism described in Ref. [37] yields a correlation of $r < 0.896$ for a quantitative analysis of the heavy-atom effect based on a plot of $\log k$ versus $\log \xi^2$, in which $k = (\tau_{5a})^{-1} - (\tau_{5b})^{-1}$ (**5x** = **5d**, **5e**, **5f**) and ξ is the spin-orbit coupling constant of the halogen atoms, because multiple processes are apparently involved in the quenching. The fact that the fluorescence-band positions of **5a** and **5e-f** are not identical hints at the influence of more than one fluorescence quenching process, since the emission band positions of the corresponding meso-tetrakis(4-halogenophenyl)porphyrin derivatives are identical within experimental error.^[41] Further evidence is provided by the longer lifetime of fluoro derivative **5c** relative to the reference compound, **5a**, which lacks a heavy-atom substituent.
- [43] A. Stone, E. B. Fleischer, *J. Am. Chem. Soc.* **1968**, 90, 2735–2748.
- [44] a) R. A. Freitag, D. G. Whitten, *J. Phys. Chem.* **1983**, 87, 3918–3925; b) A. Rosa, G. Ricciardi, E. J. Baerends, A. Romeo, L. M. Scolaro, *J. Phys. Chem. A* **2003**, 107, 11468–11482; c) C. J. Medforth, R. E. Haddad, C. M. Muzzi, N. R. Dooley, L. Jaquinod, D. C. Shyr, D. J. Nurco, M. M. Olmstead, K. M. Smith, J.-G. Ma, J. A. Shelnutt, *Inorg. Chem.* **2003**, 42, 2227–2241.
- [45] T. V. Karmanova, T. V. Gromova, B. D. Berezin, A. S. Semeikin, S. A. Syrbu, *Russ. J. Gen. Chem.* **2001**, 71, 803–808.
- [46] “Adj” and “opp” indicate the two possible isomers formed when either two adjacently or two oppositely located (dimethylamino)-phenyl groups are protonated.
- [47] R. I. Walter, E. C. A. Ojadi, H. Linschitz, *J. Phys. Chem.* **1993**, 97, 13308–13312.
- [48] E. C. A. Ojadi, H. Linschitz, M. Gouterman, R. I. Walter, J. S. Lindsey, R. W. Wagner, P. R. Droupadi, W. Wang, *J. Phys. Chem.* **1993**, 97, 13192–13197.
- [49] a) V. N. Kopranchikov, A. M. Vorotnikov, S. N. Dashkevich, E. A. Luk'yanets, *Russ. J. Gen. Chem.* **1995**, 55, 900–907; b) V. N. Kopranchikov, A. M. Vorotnikov, E. A. Luk'yanets, *Russ. J. Gen. Chem.*

- 1979**, *49*, 2758–2759; c) J. L. Retsek, C. J. Medforth, D. J. Nurco, S. Gentemann, V. S. Chirvony, K. M. Smith, D. Holten, *J. Phys. Chem. B* **2001**, *105*, 6396–6411; d) E. A. Luk'yanets, S. N. Dashkevich, N. Kobayashi, *Russ. J. Gen. Chem.* **1993**, *63*, 985–988.
- [50] a) G.-Z. Wu, H.-K. Leung, W.-X. Gan, *Tetrahedron* **1990**, *46*, 3233–3244; b) G. Hariprasad, S. J. Dahal, G. G. Maiya, *J. Chem. Soc. Dalton Trans.* **1996**, 3429–3436; c) A. Bettelheim, B. A. White, S. A. Raybuck, R. W. Murray, *Inorg. Chem.* **1987**, *26*, 1009–1017; d) C. K. Chang, J. Fajer, *J. Am. Chem. Soc.* **1980**, *102*, 848–851; e) J. Takeda, M. Sato, *Chem. Lett.* **1995**, 939–940.
- [51] K. M. Kadish, E. Van Caemelbecke, G. Royal, in *The Porphyrin Handbook, Vol. 8* (Eds.: K. M. Kadish, K. M. Smith, R. Guilard), Academic, New York, **1999**, Chapter 55, pp. 1–114.
- [52] K. M. Kadish, M. M. Morrison, *J. Am. Chem. Soc.* **1976**, *98*, 3326–3328.
- [53] C. Hansch, A. Leo, R. W. Taft, *Chem. Rev.* **1991**, *91*, 165–195.
- [54] a) G. D. Hartman, L. M. Weinstock, *Org. Synth.* **1979**, *59*, 183; b) U. Schöllkopf, D. Hoppe, R. Jentsch, *Chem. Ber.* **1975**, *108*, 1580–1592.
- [55] M. J. Plater, S. Aiken, G. Bourhill, *Tetrahedron* **2002**, *58*, 2405–2413.
- [56] Y.-H. Yu, A. B. Descalzo, Z. Shen, H. Röhr, Q. Liu, Y.-W. Wang, M. Spieles, Y.-Z. Li, K. Rurack, X.-Z. You, *Chem. Asian J.* **2006**, *1*, 176–187.
- [57] U. Resch-Genger, D. Pfeifer, C. Monte, W. Pilz, A. Hoffmann, M. Spieles, K. Rurack, J. Hollandt, D. Taubert, B. Schönenberger, P. Nording, *J. Fluoresc.* **2005**, *15*, 315–336.

Received: September 8, 2010

Revised: April 14, 2011

Published online: June 16, 2011